Quaternary International xxx (xxxx) 109878

Contents lists available at ScienceDirect

Quaternary International

journal homepage: www.elsevier.com/locate/quaint

Late Quaternary fluvio-aeolian interactions and possible aridification in west-central India: Implications for prehistoric human adaptations in the Central Tapi Valley

Sourav Mukhopadhyay [a], Pratik Pandey [a, b], Prabhin Sukumaran [a, *], Binita Phartiyal [c], Swati Verma [d], Varun Vyas [e], Navashni Naidoo [f, g], Avantika Binani [a], Jessica L. Conroy [h], Parth R. Chauhan [i]

[a] Dr. K. C. Patel Research and Development Centre, Charotar University of Science and Technology (CHARUSAT), Changa, 388421, Gujarat, India
[b] Banaras Hindu University, Ajagara, Varanasi, 221005, Uttar Pradesh, India
[c] Birbal Sahni Institute of Palaeosciences, 53, University Road, Lucknow, 226007, India
[d] Department of Archaeology and Ancient History, M. S. University of Baroda, Varodara, 39002, Gujarat, India
[e] Institute of Research and Advance Training, Universidade de Evora, Portugal
[f] Department of Anthropology, University of Illinois, Urbana, IL, 61801, United States
[g] Department of Geosciences and African Centre for Coastal Palaeoscience, Nelson Mandela University, Port Elizabeth, 6032, South Africa
[h] Department of Earth Science & Environmental Change, University of Illinois, Urbana, IL, 61801, United States
[i] Indian Institute of Science Education and Research, Mohali, 140306, Punjab, India

ARTICLE INFO

Keywords:
Microtexture
Fluvio-aeolian interactions
Central Tapi Valley
SEM

ABSTRACT

The Central Tapi Valley in India presents a unique opportunity to study Late Quaternary environmental changes, with a particular focus on fluvio-aeolian interactions, aridification, and their implications for human adaptation. To reconstruct the sedimentary history, we used a multi-proxy approach using microstructural analysis of quartz grains, grain size distribution and magnetic susceptibility. Our findings reveal a two-phase depositional process, where aeolian influences dominate the lower layers and fluvial processes prevail in the upper layers, suggesting seasonal wind variations and episodic aridification in the region. In the magnetic susceptibility data Phase-1 is characterized by ferrimagnetic minerals linked to increased pedogenesis and intensified Indian Summer Monsoon activity, and the Phase-2, dominated by antiferromagnetic minerals indicative of aeolian processes and drier conditions. These findings underscore the broader patterns of intercontinental aridification, extending into central India and influencing human habitation and adaptation strategies during this period. Hence this study contributes to the understanding of the Late Quaternary landscape transformations and provides valuable insights into how climate variability and environmental stressors shaped human adaptation in West-Central India and demonstrates the potential to enhance the understanding of intercontinental aridification and dustiness in central India, reaching beyond the Himalayan and Thar Desert zones.

1. Introduction

The migration and adaptation of prehistoric *H. sapience* to South Asia have been subjects of debate for several decades. Environmental, archaeological, fossil, and genetic data provide inconsistent models, suggesting that the prevailing "Out of Africa" hypotheses may be oversimplified or underestimated (Groucutt et al., 2015). However, the academic community acknowledges that new fossil evidence from South Asia has the potential to transform our understanding of prehistoric *H. sapiens* migration and adaptation, offering insights into the role of climate and environmental changes in demographic distributions across the region (Dennell, 2021; Groucutt et al., 2015). In the absence of definitive fossil evidence from the Indian subcontinent, a viable approach involves integrating regional process correlations with archaeological and genetic data. Despite this, a significant disconnect exists between archaeological records and geological studies in the region. As a result, many well-documented archaeological sites lack comprehensive geological context, while geological studies often remain detached from ar-

This article is part of a special issue entitled: Landscape change & human adaptation in the drylands published in Quaternary International.

* Corresponding author.
E-mail address: prabhinsukumaran.cv@charusat.ac.in (P. Sukumaran).

https://doi.org/10.1016/j.quaint.2025.109878
Received 24 October 2024; Received in revised form 31 May 2025; Accepted 8 June 2025
1040-6182/

chaeological frameworks. Addressing this gap requires a concerted effort toward geoarchaeological research to refine our understanding of paleoenvironments in the Indian subcontinent (Mehra and Chauhan, 2021).

Studying Quaternary deposits in the monsoon-dominated Indian subcontinent poses significant challenges from a geoarchaeological perspective. Pleistocene sediment sequences are frequently buried beneath extensive terrestrial deposits, and the dominance of modern geomorphic processes often obscures or overprints earlier sedimentary records. Consequently, multiple phases of environmental change—particularly those reflected in aeolian sediments—are frequently overlooked or understudied. For instance, the reported presence of 20–30 m thick loess deposits in the Son Valley (C^{14} dated between 25 kyr and 3 kyr), likely sourced from the Ganga Basin or the Thar Desert, presents a promising archive for investigating prehistoric land use and early agricultural practices (Williams and Clarke, 1984). However, despite its potential, this deposit has not been the focus of sustained research.

Fluvial-aeolian interactions in the Thar Desert (TD) have been interpreted as indicative of a dynamic interplay between monsoonal variability and arid phases (Blinkhorn et al., 2017, 2020; Kar et al., 2001). However, similar interactions occurring beyond the TD, particularly in the Gujarat Alluvial Plain (GAP), remain underexplored in an archaeological context, despite the availability of chronological data (Chamyal et al., 2002; Chauhan and Morthekai, 2017; Juyal et al., 2000; Merh and Chamyal, 1993). From a morphostratigraphic perspective, aeolian deposits in both the TD and GAP typically overlie older fluvial sequences (Chamyal et al., 2002; Chauhan and Morthekai, 2017; Juyal et al., 2000; Merh and Chamyal, 1993). Consequently, the transition from arid aeolian phases to wetter fluvial phases is often masked by erosional processes, limiting our ability to reconstruct prehistoric human adaptations to these environmental shifts.

The Central Tapi River Valley (CTRV) occupies a pivotal position in this discussion due to its geomorphic setting and rich archaeological record spanning multiple cultural phases (Sali, 1985, 1989, 1990; Sukumaran et al., 2023b). The Tapi River, extending ~724 km (Fig. 1), is the second-largest (after Narmada) west-flowing interstate river in peninsular India. Situated in the northern Deccan Plateau, the valley is enclosed by hill ranges to the north, east, and south, while to the west, it flows into the Arabian Sea via the Gujarat Alluvial Plain (GAP). The valley lies approximately 100 m above the GAP and ~400 km SSW of the present-day Thar Desert boundary (Fig. 1a and b). Lithologically, the region is underlain by Deccan Trap basalt, with minor exposures of Pre-Cretaceous formations in its northeastern margins (Fig. 1 c).

Archaeological excavations and Quaternary sediment studies in the CTRV have previously suggested an association with aeolian processes in semi-arid settings (Sali, 1985), while some natural exposures across the broader Deccan region have been linked to neotectonic activity (Malik, 1996). A regional survey of exposed sections, spanning from foothill regions to the main river channel, combined with the discovery of a ~47,000-year-old ostrich eggshell fragment, tentatively supports the hypothesis of an arid to semi-arid climatic regime in the valley during the Late Pleistocene (Sukumaran et al., 2023b). However, a substantial research gap persists due to the limited availability of high-resolution empirical and instrumental data required to validate these interpretations. The present study seeks to bridge this gap by systematically evaluating the hypothesized presence of aeolian sediments in the Sakegaon section through a multi-proxy approach, incorporating quartz grain surface microtexture analysis, grain size distribution, and magnetic susceptibility measurements.

Surface microtextures of quartz grains serve as valuable indicators of depositional processes, as their morphologies are influenced by transport mechanisms and prevailing climatic conditions (Hu et al., 2023; Kemnitz and Lucke, 2019; Smith et al., 2018; Vos et al., 2014).

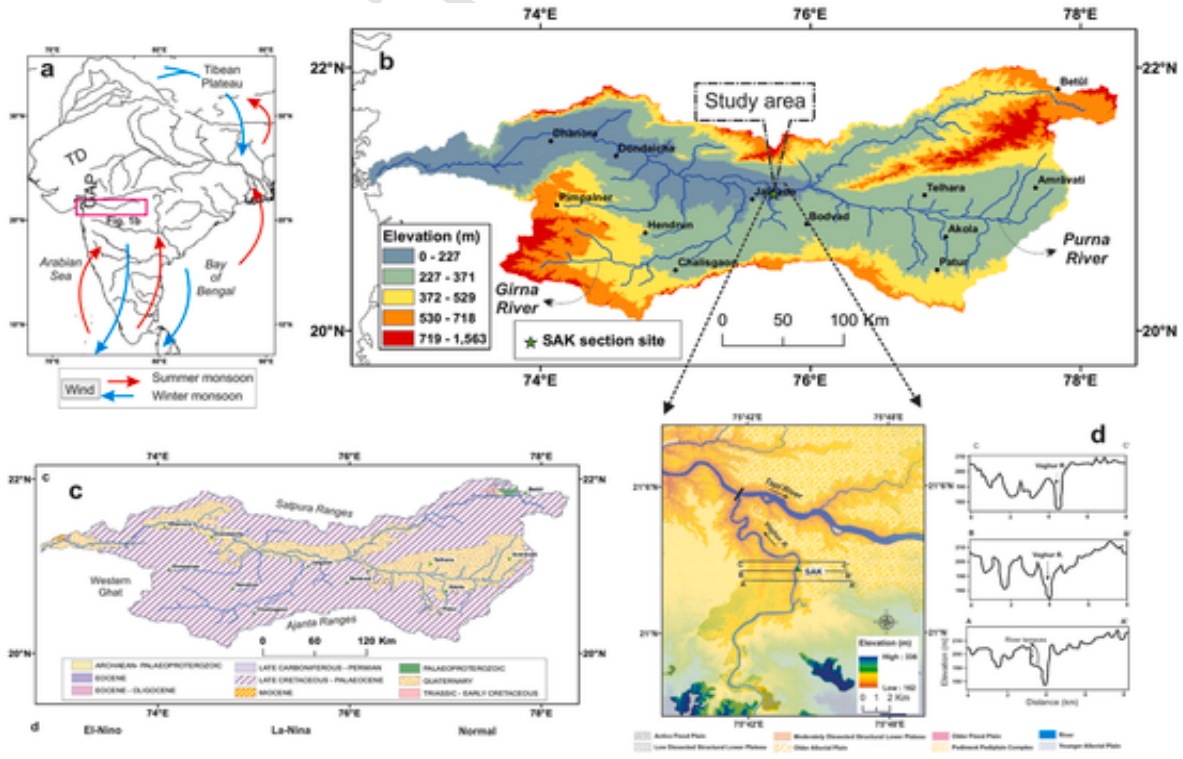

Fig. 1. Location map of the study area (a) The geographic location of the study area. (b) A digital elevation map of the Tapi Basin and the SAK section location in the central Tapi Valley. (c) A simplified geological map of the Tapi River Basin along with major drainage (vector data are from https://bhukosh.gsi.gov.in)., (d) Topographic and geomorphic classification of Sakegaon landform.

These microtextures have been widely applied to distinguish among fluvial, aeolian, marine, glacial, and lacustrine depositional environments (Cardona et al., 2005; Chmielowska and Woronko, 2019; Krinsley and Donahue, 1968; Li et al., 2020; Marshall et al., 2012; Smith et al., 2018; Vos et al., 2014). The interpretative framework developed by Vos et al. (2014) for distinguishing between these environments based on quartz microtextures has been instrumental in paleoenvironmental reconstructions. Additionally, mineral grains such as quartz and ilmenite retain microtextures that provide insights into soil formation, depositional processes, and paleoenvironments (Mahaney, 2002). Despite these advances, there remains no universal consensus on which microtextures are uniquely diagnostic of specific depositional environments (e.g. Costa et al., 2013). This study contributes to this ongoing discussion by integrating microtextural analysis with complementary sedimentological and geochemical proxies to refine our understanding of Late Quaternary fluvio-aeolian interactions and their implications for prehistoric human adaptations in the Central Tapi Valley.

2. Regional background

The present study investigates the textural and compositional variability of Quaternary deposits of a stratigraphic section at Sakegon (SAK), which is located in the middle reaches of the Tapi Valley (Fig. 1 b) in west-central India. The thick yellowish-colored bluff fine sand and silty-clay sediment is seen in the region overlying the Cretaceous–Eocene basalt basal rocks. The Quaternary sediment thickness increases upland (more or less 14 to 10 m), hypothesizing an aeolian source, but uncertainties remain regarding the source (derived and deposited locally); the geochemical process responsible for basaltic weathering to produce this yellow silt and its implication or link to hydroclimatic change. Alternately, if the yellow silt sediments are not local, and are brought to the valley by a process other than fluvial activity, there is potential to decode the regional changes in aridification and atmospheric circulation. Hence, the source area and deposition environment of such a deposit has a potential for a detailed assessment.

The section site (Fig. 1b) near Sakegaon village is located at coordinates 21° 3′ 17.13″N, 75° 44′ 6.61″E elevation 205 m from MSL, on the right bank of the Vaghur River, a tributary of Tapi River. It is situated ~7 km to the southern direction of the Shelgaon Barrage on Tapi River and is ~1 km north-west from Sakegaon village, affected by the most substantial inundations during the monsoonal time. The cultivated fields are situated at an elevation of 5–10 m above the flood level and 20 m above the present day Tapi river base level.

3. Methodology

3.1. Fieldwork and sample collection

Regional geomorphic mapping of Quaternary deposits in the central Tapi river valley has been carried out with the help of Google Earth and Landsat-8 satellite images, which reveal a distinctive landform near Sakegaon village as documented by Sukumaran et al. (2023b). The relict eroding landform in the older alluvial surface, situated between the Tapi main river channel and its tributary Vaghur, exhibits an elevation range from 192 to 207 m above mean sea level (msl), covering an area of ~165 km^2 in the Sakegaon region. The Quaternary sequence unconformably lies over the Deccan Trap basalt rock. The landform is beyond the reach of river bank full stage and it is separable from the active flood plain, classifying it to older flood plain (Fig. 1d). Over the past few years, extensive soil excavation for construction purposes has exposed numerous vertical sections, which aided in selecting the site for the step trench. The basal unit of these sections consists of a finer silt facies that grades into a sequence intercalated with sand, silt, and clay in the upper portion. A comparative facies analysis in the other sections was also done to enable a comprehensive understanding of the landform's composition. All sampling was conducted from a freshly cut, newly opened step trench that extended down to the bedrock (basalt) to ensure minimal disturbance. Sampling at a 2-cm-interval was done for a ~14 m thick sedimentary sequence at SAK in the year 2021 (Fig. 2). Approximately 600–700 g of bulk sediment (n = 695) samples were collected, labelled and packed in air-tight sample bags until subsequent analysis.

3.2. Laboratory processing

All the collected samples were examined in the laboratory under natural light, and their visual and textural characteristics (general size range and general sorting), presence or absence of organic residues, and calcrete nodules were documented. All 695 samples were analysed for magnetic susceptibility (high frequency, low frequency and frequency dependency) analysis. Subsequent to the magnetic susceptibility analysis and visual interpretation of sediment characteristics, a generalised litholog was prepared and five units were distinguished. Nine representative samples (from those five units) were taken for grain size and microstructure analysis (Table 1) (see Table 2).

3.2.1. Grain size analysis

Particle size distribution was determined using Malvern Mastersizer 3000 instrument in the Department of Earth Science & Environmental Change, University of Illinois, Urbana, USA. Following a standard pretreatment (HCl and H_2O_2 treatment) to remove carbonates and organic matter, a 15–20 ml of distilled, deionized water was added to each sample. The sample was then vortexed for 20 s, shaken vigorously, and added to a HydroMV dispersion unit attached to the Mastersizer to achieve an obscuration range between 10 and 20 %. The HydroMV was set to 3500 rpm per minute, with 20 % sonication for 1 min prior to measurement. An in-house standard of Illinois River Valley Loess was measured to test instrument precision once per day. Each sample was measured 5 times and the average is reported as grain size diameter volume percent abundance. GRADISTAT software (Blott and Pye, 2001) packages were used to calculate and define grain-size parameters, e.g., mean grain size (ME), which measures the average size of the sediment; standard deviation (SD), which measures the spread of the distribution around the mean and shows how the sediment is sorted; skewness (SK), measures the symmetry of distribution around the mean; sorting index (SI), which represent the how grains are shorted over the sample population size and kurtosis (KS) measures of the peakedness of the distribution.

3.2.2. Low-field magnetic susceptibility (χ_{lf}) and frequency-dependent susceptibility (χ_{fd}) measurement

All samples (n = 695) were air dried and packed in standard non-magnetic plastic bottles of 10 cm^3. Low magnetic susceptibility (χ_{lf} at 976 Hz) and high (χ_{hf} at15616 Hz) frequency was determined by a Multi-Function Kappabridge (MFK1-FA) sensor at Palaeomagnetism laboratory, Birbal Sahni Institute of Palaeosciences, Lucknow, India. To quantifying the range of magnetic susceptibility in terrestrial sediment offers useful insights into processes such as weathering, sediment transport, and changes in source material. This information is crucial for recreating past environmental conditions (Evans and Heller, 2003; Panwar et al., 2020; Sangode et al., 2007; Sinha et al., 2007b). For qualitative and quantitative estimates of fine grained superparamagnetic (SP) particles, we used the frequency-dependent susceptibility [$\chi_{fd} = (\chi_{lf}-\chi_{hf})/\chi_{lf}$], which is defined as the value usually recognized as characterized by- Dearing et al. (1996).

3.2.3. Sample selection and Scanning Electron Microscopy (SEM) study

The investigation consisted of four fundamental phases: reconnaissance, sample selection, preparation, SEM analysis, and then statistical data analysis. In the present study, quartz grains from nine representa-

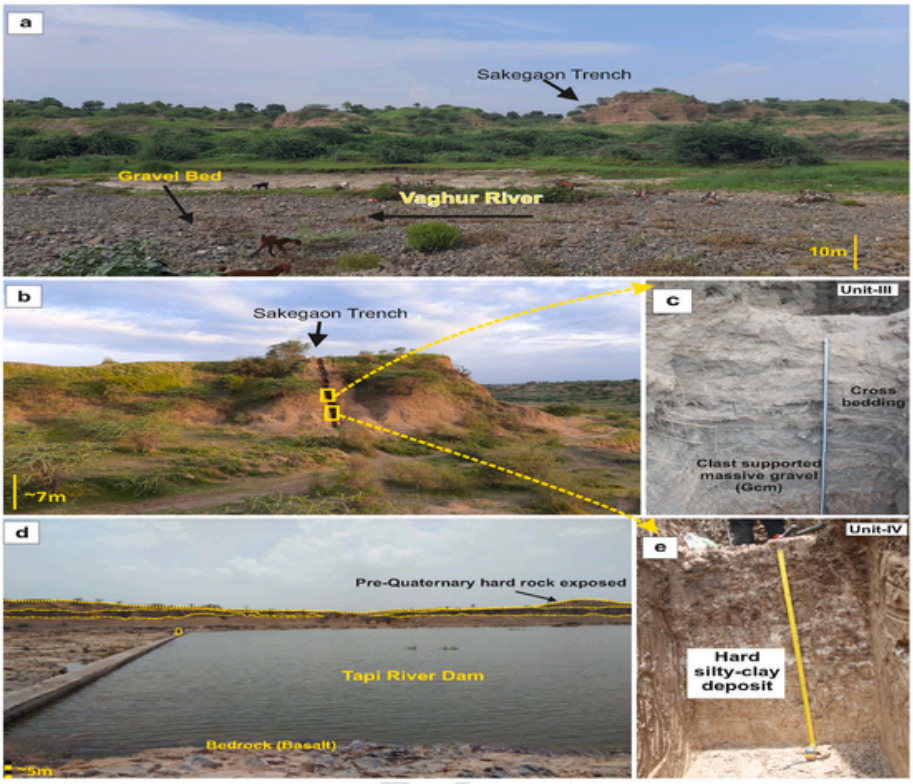

Fig. 2. Field Photographs. (a) Field photographs showing the different pockets of Quaternary deposit on near the Vaghur River (a tributary of Tapi River). (b) The Sakegaon (SAK) fluvial deposit is perched on the older bedrock surface. (c) Photograph showing Unit-3of the SAK section, where cross bedding and massive gravel layers are prominent feature. (d) Dam site photographs showing (before monsoon) the Basaltic bedrock surface in the Tapi River Valley. (e) The stratigraphic contact relationship of the Tapi alluvial sequence and hard silty-clay showing a continuous extensional stratum of the hard silty-clay with the lower part of the SAK section.

Table 1
Unit-wise description of Quaternary deposits in the Sakegaon section, Central Tapi Valley.

Si No.	Unit	Depth (cm)	Sample Number (Depth cm)	Mean as per Gradistat analysis (Blott and Pye, 2001)
1.	Unit 1	0–70	SAK001 (1 cm)	Coarse Silt
2.	Unit 2	71–251	SAK085 (169 cm)	Very Fine Sand
3.	Unit 3	252–745	SAK165 (329 cm)	Very Fine Sand
			SAK245 (489 cm)	Very Fine Sand
			SAK325 (649 cm)	Very Coarse Silt
4.	Unit 4	746–1171	SAK405 (809 cm)	Medium Silt
			SAK485 (969 cm)	Medium Silt
			SAK565 (1129 cm)	Medium Silt
5.	Unit 5	1172–1389	SAK645 (1289 cm)	Coarse Silt

tive samples (e.g., SAK001, SAK085, SAK165, SAK245, SAK325, SAK405, SAK485, SAK565 and SAK645) from the distinct five distinct units were collected. A large grain-size range should show a larger range of textures; as different textures can be more or less prevalent depending on grain size. Previous studies (Mahaney, 2002) of microstructure analysis advocated various approaches on grain size selection and number of grains to be selected from each sample (Table 2). Sand was first isolated by gently wet sieving the bulk sediment samples, following the acid treatment steps to remove the carbonates, organic (algal) matter and any other iron-oxide and manganese-oxide coatings from the quartz grains (see details in supplementary file). Sub samples of each representative samples were prepared for SEM analysis, following

Table 2
Previous studies demonstrating varying sample sizes and their corresponding fractionation values.

Reference	Number of grains studied/sample	Grain size fractionation used
Present study	42 to 66	63–255 μm 45–63 μm
Smith et al. (2018)	50	250 μm -1mm
Armstrong-Altrin and Natalhy-Pineda (2014)	20	200–400 μm
Vos et al. (2014)	10–15	100–2000 μm
Immonen (2013)	30	250–600 μm
Keiser et al. (2015)	20–40	250–1000 μm
Costa et al. (2012)	15–20	125–500 μm
Deane (2010)	>100	150–250 μm
Sweet and Soreghan (2010)	10–55	300–3000 μm
Chakroun et al. (2009)	10	300–500 μm
Alekseeva (2005)	50–60	250–500 μm
Mahaney (2002)	20	250–500 μm; 500–2000 μm
Mahaney and Kalm (2000)	25	63–2000 μm
Helland et al. (1997)	35–40	200–1000 μm

the method suggested by Vos et al. (2014). Quartz grains (each stub held ~45–65 grains) were mounted on aluminum stubs and coated with platinum, before using the scanning electron microscope (JEOL 6010LA SEM at 15 to 5 kV) at Dr. K. C. Patel Research and Development Centre, Charusat University.

3.2.4. Micro-structure and shape analysis

We documented the microtextures on each grain by recording the presence, absence, and abundance of 34 surface textures, followed by the procedure by Vos et al. (2014). Each grain SEM image was visually analysed and classified according to the presence of 34 main microtextural features and grouped them in to mechanical (M), chemical (C), and both mechanical-chemical (MC) weathering characteristics. The shape of each grain was analysed using the freeware ImageJ v1.49 (see Schneider et al., 2012). ImageJ was used to determine the shape factors, such as circularity, aspect ratio, and roundness. Grain roundness was calculated by dividing the largest inscribed circle's radius by its mean radius of curvature (Wadell, 1932). The roundness parameter of each grain was calculated, followed by methods established by Takashimizu and Iiyoshi (2016).

3.2.5. Statistical analysis

The present study uses 34 microstructural parameters for 482 quartz grains. All 34 microtexture parameters were considered together in the first step. The subsequent stage analysis successfully considered only the 19 mechanically (M) induced microtextures. Analyzing this data and interpreting the depositional environment from the database is substantially challenging, considering that no single microstructure can be a crucial identification feature for a specific deposition environment. Over and above, multiple generations and over-printing of microstructure are expected in a dynamic environmental setup like a fluvial system. In such a situation, it is crucial to decipher statistically significant microstructure from the dataset. Principal Component Analysis (PCA) and cluster analysis were applied to explain the microstructure and sample variation. PCA is one of the robust techniques used for adaptive description data analysis, in many variable datasets (Jolliffe and Cadima, 2016). The method is necessary to substantially reduce the dimensionality of such datasets in an interpretable manner so that the majority of the information contained within the data can be captured. The examination of each data set yielded a collection of plots that depict the correlation between various variables, primarily microtexture fracture, and with each principal component. The present study conducted PCA to reduce the number of variables required to explain the majority of variance in the data by identifying a new set of variables (principal components) and prioritizing those variables in order of their statistical variance.

4. Results

4.1. Lithology and grain-size analysis

The study analyses different facies based on field observations, considering lithological composition, grain size of individual units, geometry of the sediment body, and sedimentary structures. Sediment name-Fine Sand (FS), Very Fine Sand (VFS), Very Course Silt (VCS), Course Silt (CS) and Medium Silt (MSi)- were assigned to the samples biased on descriptive terminology of mean grain size from the GRADISTAT package (Blott and Pye, 2001). The upper and lower boundaries of each sediment unit were determined through field observation and a generalised ~14 m litholog was prepared to describe the facies (Table 1and Fig. 3). The section is divided into two broad depositional phases, separated by by a distinct disconformity at 733 cm (Fig. 3). Phase 1 (Upper) has three identified units (Unit 1, 2 and 3) and Phase 2 (lower) has two distinct units (Unit 4 and 5).

The base of the Phase 1 sediment sequence unconformably overlies the Phase 2 sediment sequence. The sequence is predominantly composed of four sediment groups, namely FS, VFS, VCS, and CS. The lowermost part of Phase 1 comprises Unit 3, an intercalated sequence of all four sediment groups with a 70 cm thick cross-bedded layer (Fig. 2c). The cross-bedded lower layers of Unit 3 gradually transition into an intercalated sequence of FS, VFS, and VCS. Visible fine laminations can be seen in the FS and VFS layers of the unit. The transition from Unit 3 to Unit 4 is gradual, with an increased thickness of the VFS layer, without any visible sedimentary structures. Pedogenetic calcrete nodule formation has been observed in the upper part of Unit 3 through the lower part of Unit 2.

The uppermost unit of Phase 1, Unit 1, is an intercalated sequence of VCS and CS. Carbonate nodule formation is visible across the boundary from the upper part of Unit 2 through the lower part of Unit 1. Both Unit 2 and Unit 1 are devoid of any sedimentary structures.

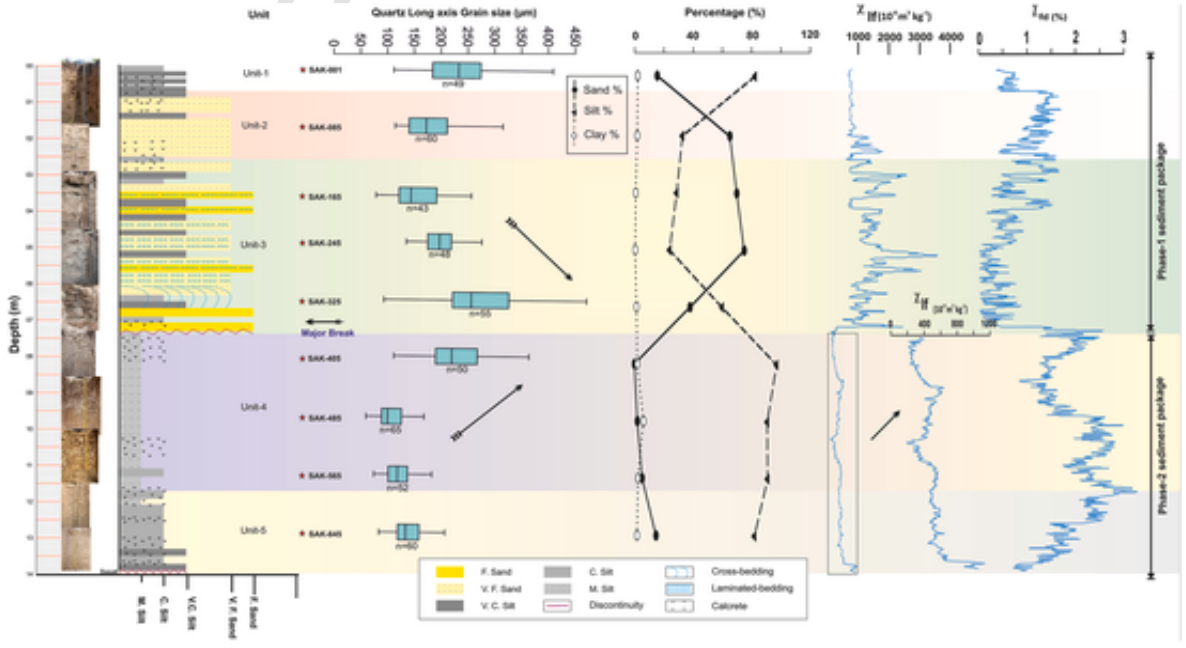

Fig. 3. A simplified lithostratigraphy of the Sakegaon sequence with SEM sample location, showing sand, silt and clay percentages, along with comparison of the sedimentary characterand magnetic susceptibility.

Phase 2 is predominantly a silt sequence, with VCS- and CS-dominated Unit 5 and MSi-dominated Unit 4 (Fig. 2e). Unit 4 is distinguishable from the lower Unit 5 by a pedogenetic layer developed at a depth of 1170 cm. Both Unit 4 and Unit 5 are characterized by minor basal gravel. Field-based physical examination indicates significant variation in the percentage and type of calcrete formation in these units. Unit 4 has calcrete precipitation across its depth but is characteristically chalky, with nodule formations at two horizons (1160 cm–1200 cm and 1240 cm–1262 cm). In contrast, Unit 5 features calcrete nodule formation distributed throughout its depth.

Grain size analysis of nine representative samples (refer to Fig. 3 and supplementary file Fig. S1) from different units aids in distinguishing sedimentary settings and transport dynamics. Grain-size parameters as outlined by Folk and Ward (1957), including mean size, sorting, skewness, and kurtosis were analysed (see Table 3). All representative samples exhibit poor sorting characteristics with sorting coefficient ranges from 1.42 Φ to 2.68 Φ in Phase-1 and 1.21 Φ to 1.57 Φ in Phase-2. Notably, the sample from Unit 3 (depth at 649 cm; SAK325) displays a very poorly sorted value of 2.68 Φ, indicating a significant transition between Phase 1 and Phase 2 sedimentation processes. Phase-1 samples display either unimodal or bimodal distributions, whereas Phase-2 samples predominantly exhibit unimodal distributions.

Other textural characteristics of the sediments from the SAK section include mean size, sorting, skewness, kurtosis, D10, D50, and D90 (see Table 3; supplementary file Fig. S2). The mean grain size of the SAK section samples varies between 3.56 Φ to 6.63 Φ. Phase-1 exhibits a range of coarse-grained deposits, while Phase-2 is predominantly fine-grained. The calculated skewness values for the samples range from −0.28 Φ to 0.52 Φ and from 0.1 to 0.3 Φ. Kurtosis values for the studied samples range from 0.60 Φ to 1.56 Φ and from 0.83 to 1.09 Φ, representing a spectrum from platykurtic to leptokurtic distributions. Mineral Magnetic (χ_{lf} and $\chi_{fd\%}$) Data

Fig. 3 illustrates the magnetic susceptibility (χ_{lf}) plot depicting relative variations across two distinct phases. The χ_{lf} values range from 179 to 3929 × 10^{-8} m^3 kg^{-1}, indicating significant variability. Maximum χ_{lf} occurs at Unit 2, while minimum values are observed at Unit 4 (refer to Table 4). Unit 4 exhibits weak susceptibility, ranging from 179 to 634 × 10^{-8} m^3 kg^{-1}, with the average value is 413 × 10^{-8} m^3 kg^{-1} χ_{lf} values undergo substantial changes with depth, increasing from ~700 - 800 × 10^{-8} m^3 kg^{-1} in Unit 1, to about 600–1900 × 10^{-8} m^3 kg^{-1} in Unit 2, and exceeding 3929 × 10^{-8} m^3 kg^{-1} at 512 cm depth in Unit 3. Exceptionally high χ_{lf} values are observed between 5.2 and 7.1 m depth in Unit 3, attributed to the presence of biogenic fine-grained materials dominated by Deccan basalt and pedogenesis processes.

The χ_{fd} and $\chi_{fd\%}$ parameters, help identify very small magnetic particles that are close to the superparamagnetic (SP) or single domain (SD) threshold (Dearing et al., 1996; Liu et al., 2012). χ_{fd} values ranging from ~0.02 to 3.26 × 10^{-8} m^3 kg^{-1} indicate significant concentrations of SP magnetic particles. $\chi_{fd\%}$ fluctuates similarly to χ_{lf} results, generally decreasing with depth (1–3 %). In Unit 1, $\chi_{fd\%}$ varies from 0.4 to 1.5 % increasing to 0.40–1.68 % in Unit 2, Relatively lower values are observed in Unit 3. Unit 4 exhibits elevated $\chi_{fd\%}$ values in its middle section (0.82 %–3.26 %). Unit 5 shows a decreasing trend from 0.7 to 2.7 %. The highest mean $\chi_{fd\%}$ value of 2 % is noted in Unit 4, corresponding to Phase 2 cycle.

4.2. Quartz microtexture analysis

The shape and surface characteristics of the quartz grains in the sediment fraction can give a detailed nature of the mechanisms causing sediment deposition (Kalińska and Nartišs, 2014; Mahaney, 2002). In the SAK lithounit, the grain roundness is varying from Phase 1 to phase 2; where, Unit 1 to Unit 3 show average value of 0.31 and in Phase-2; Unit 4 and Unit 5 is 0.39 (supplementary file Fig. S4), which indicates more roundness compared to Phase 1. Fig. 4a shows that maximum amount of grains belongs to roundness range from 0.16 to 0.40. The box diagram (Fig. 4b) represents the variation in the grain roundness, where the minimum mean value is noticed in SAK165 (depth at 329 cm; Unit 3) and maximum value is noticed in sample SAK645 (depth at 1129 cm; Unit 5). From the study, it is evident that grain-size controlled intra-sample variability of grain roundness is minor, but the roundness values change slightly from the top to the middle and bottom of the section (Fig. 4 a).

4.2.1. Phase-1 sediment package (Unit 1, 2, and 3)

Each SEM image of quartz grains underwent visual analysis and classification based on the presence of 34 primary microtextural features (refer to Figs. 5–7 and 8). Within the Phase-1 package, the majority of quartz microtextures shared across all units are angular to subangular (>75 %) and exhibit abrasion fatigue (52–75 %). Grains displaying medium relief are prevalent in Phase-1, constituting 63 % in Unit 1, 40 % in Unit 2, and an average of 38 % in Unit 3. Conversely, grains with high relief and angular shapes are infrequently identified in this phase.

From Unit 1 most common features are angular outline (91 %), abrasion fatigue (>80 %), solution pits (81 %), elongated depressions (91 %). Unit 2 represents sub-angular outline (>90 %), graded arcs (68 %), abrasion fatigue (80 %) and low relief (45 %). Unit 3 shows angular outline (>78 %), abrasion fatigue (54–82 %), solution pits (>70 %, Fig. 7c), abrasion fatigue (>50 %), solution pits (>70 %) and ar-

Table 3
Summary of statistical measures of grain-size distributions at the Sakegaon (SAK) section.

Sample No	Unit	Sample Depth (cm)	Sand %	Silt %	Clay %	Sample type	Mean (ϕ)	Sorting (ϕ)	Skewness (ϕ)	Kurtosis	D10 (ϕ)	D50 (ϕ)	D90 (ϕ)	Mean Roundness
SAK001	Unit-1	1	15.5	82.4	2.1	Unimodal, Poorly Sorted	5.46	1.62	0.22	1.16	4.36	27.45	80.43	0.29
SAK085	Unit-2	169	65.3	32.8	1.9	Unimodal, Poorly Sorted	3.78	1.42	0.39	1.41	14.68	86.40	183.49	0.30
SAK165	Unit-3	329	70.1	28.9	1.0	Bimodal, Poorly Sorted	3.60	1.80	0.52	1.13	9.98	122.12	263.62	0.25
SAK245		489	75.2	24.2	0.6	Bimodal, Poorly Sorted	3.55	1.56	0.49	1.55	13.83	114.95	232.15	0.35
SAK325		649	38.2	60.2	1.6	Bimodal, Very Poorly Sorted	4.68	2.68	−0.28	0.59	4.26	23.33	484.33	0.37
SAK405	Unit-4	809	0.3	97.5	2.2	Unimodal, Poorly Sorted	6.63	1.21	0.06	0.93	3.20	10.45	28.88	0.38
SAK485		969	2.3	91.2	6.5	Unimodal, Poorly Sorted	6.59	1.57	0.06	0.83	2.41	10.79	40.10	0.39
SAK565		1129	5.7	91.5	2.8	Unimodal, Poorly Sorted	6.23	1.47	0.05	0.96	3.35	13.80	47.37	0.29
SAK645	Unit-5	1289	15.2	82.6	2.2	Unimodal, Poorly Sorted	5.33	1.46	0.33	1.09	5.08	30.12	72.47	0.38

Table 4
The table presents unit-wise statistics of magnetic susceptibility, along with correlation values between χ_{lf} and χ_{fd}.

Parameter	Unit 1 (n = 35)	Unit 2 (n = 100)	Unit 3 (n = 240)	Unit 4 (n = 215)	Unit 5 (n = 105)
χ_{lf} Min	752	689	195	179	442
χ_{lf} Max	891	1982	3929	634	1137
χ_{lf} Mean	830	1012	1472	413	597
χlf Stand. dev	42	282	670	108	156
χ_{lf} Median	833	873	1418	433	546
Coeff. Var	5.12	27.92	45.51	26.12	26.04
χ_{lf} vs χ_{fd} Correlation (r^2) value	0.12	0.66	0.43	0.01	0.52

cuate/circular/polygonal cracks (>50 %). While numerous small and medium pits are evident in the samples, there is a scarcity of large pits on the grains.

In Phase-1, quartz grains exhibited irregular pits and conchoidal fractures of varying sizes, with small to medium conchoidal fractures being predominant, constituting nearly 35 % of observed fractures (particularly evident in Unit 3; see Supplementary Fig. S5) within this package cycle. Mechanically upturned plates and V-shaped pits were either common or sporadic in the Phase-1 package, with a higher frequency (>65 %) observed in Unit 1, while other units displayed a sparse occurrence.

All quartz grains from this Phase-1 package displayed microtextures attributable to chemical breakdown or precipitation processes. Chemical microtextures observed (as shown in Fig. 5) included oriented etch pits and solution pits, with frequencies of 65 % and 81 % in Unit 1,

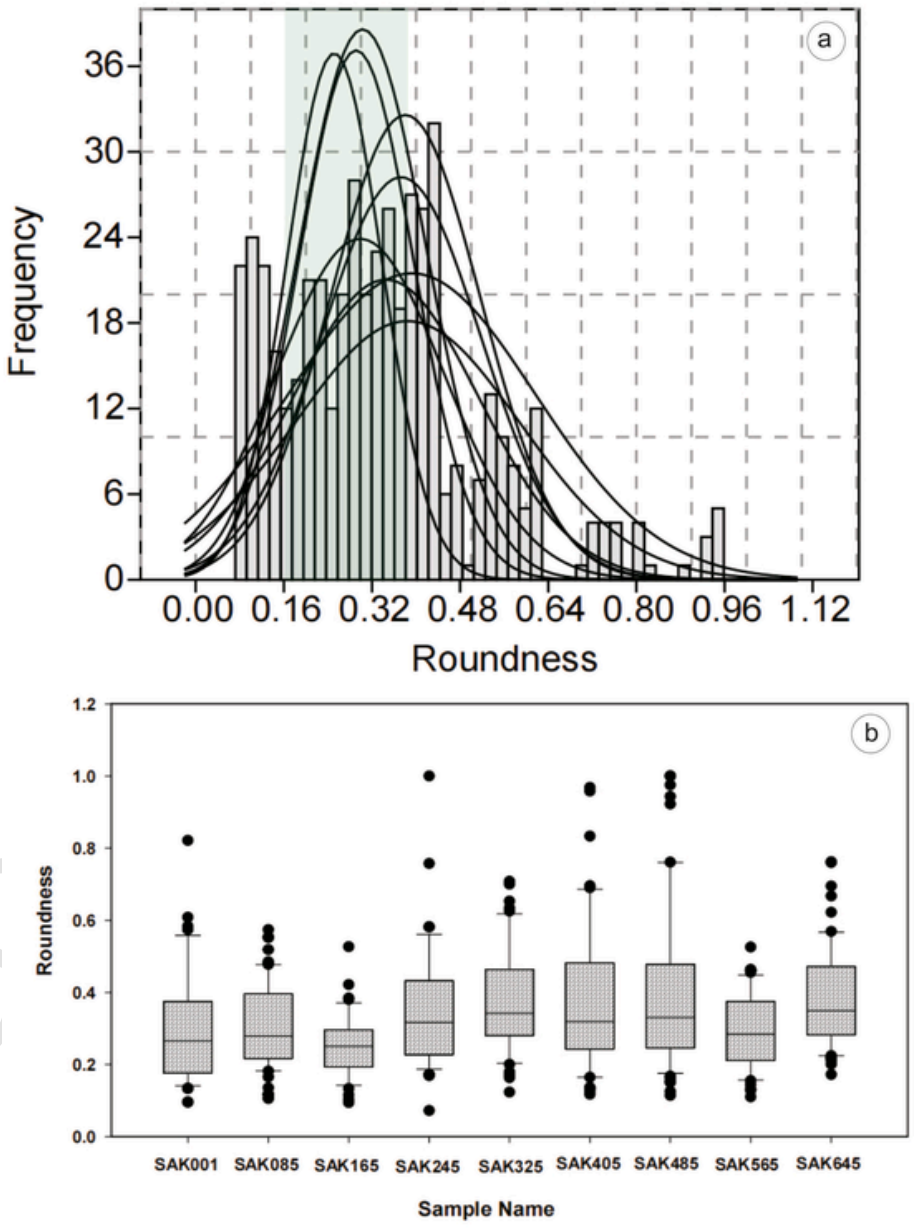

Fig. 4. a. Histogram graph showing the SAK grain roundness range categories, which shows the maximum roundness values shows between the ranges of 0.3–0.4 were preferred. b. Box plot diagram showing the roundness of the intra-sample variability in fluvial (Unit 1, 2 and 3) and aeolian (Unit 4 and 5) sands of SAK section (Black dots represent the outlier).

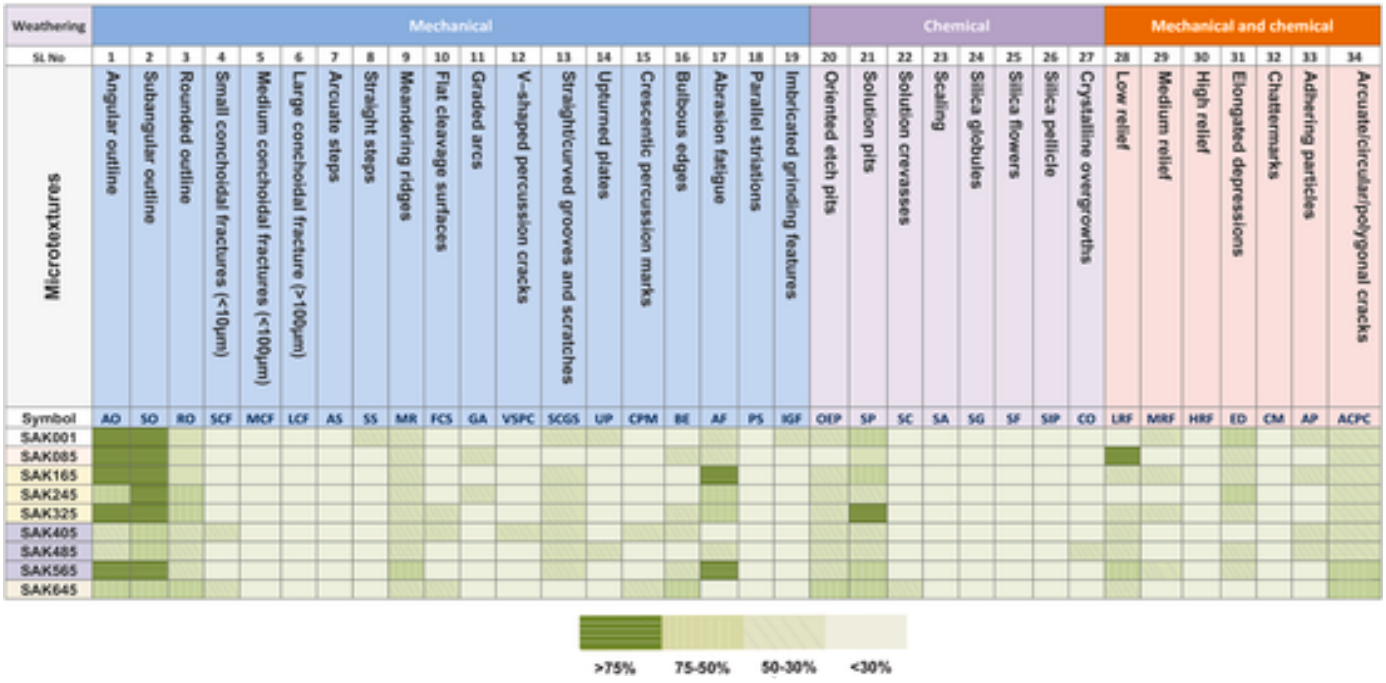

Fig. 5. The table diagram showing the different microstructure features in the quartz grains. "Abundant" means that the feature is present on >75 % of the grains, "common" 75–50 %, "sparse" 50–30 %, and "rare" <30 %; (for more details of the microstructure abbreviations, see Table no 6).

28 % and 48 % in Unit 2, and ranging between 40 and 60 % and exceeding 80 % in Unit 3. Notably, microtextures formed by chemical precipitation, such as silica pellicle, silica flowers, and crystalline overgrowth, were not abundant on the quartz grains.

4.2.2. Phase-2 sediment package (Unit 4, and 5)

The second phase of sediment package clearly shows nine main microtextural features found on the grain surfaces (see the common features in Fig. 8). All common microstructure and their percentages range are subangular outline (80–90 %), rounded outline (70–80 %), flat cleavage surfaces (17–60 %), bulbous edges (9–86 %), meandering ridges 55–82 %), oriented etch pits (50->90 %), solution pits (69–95 %), low relief (61–83 %) and arcuate/circular/polygonal cracks (67–86 %). Sub angular grains with sharp edges from the Phase 2 samples, accounted for >45 % and maximum rounded outline (30 %) grains are present in both the units. The flat cleavage surfaces were on an average 42.3 % in Unit 4 and 68.33 % in Unit 5 in Phase-2 package. Bulbous edges and meandering ridges exhibit varying frequency distributions, with a higher occurrence (85 %) of bulbous edge features observed in Unit 5, while meandering ridges are more prevalent (averaging 72.3 %) in Unit 4. V-shaped percussion cracks are sparse, and grains with parallel striations are found in less than 10–20 % of this phase. Notably, the highest concentration of crescentic percussion marks is found in sample SAK-405 (at a depth of 809 cm; Unit 4).

Chemical microtextures such as solution pits and etched pit (Fig. 8B) surfaces are prevalent in most quartz grains within this sediment package, with frequencies ranging from 69 % to 85 % in Unit 4 and exceeding 90 % in Unit 5. The distribution of both mechanical and chemical microtextures of fracture plates/planes in the quartz grains is limited (see Fig. 5). Quartz grains exhibit varying relief, including low, medium, and high. Unit 4 displays high relief, with a prevalence of over 15 %, whereas Unit 5 exhibits a low occurrence (3 %) of high relief, with low relief being nearly equal in both units.

4.2.3. Comparison between Phase-1 and phase 2

A comparative analysis of microstructural features from SAK section reveals the Phase-2 is dominated by features such as meandering ridges, upturned plates, and bulbous edges. The meandering ridges at the Unit 4 and 5 (SAK405, SAK485, and SAK645) is described as an indication of process like coastal and desert dune sands (Mejía-Ledezma et al., 2020; Silpa et al., 2016). Upturned plates on quartz grain (>35 %observed in SAK485 samples from Unit 4) are a prominent feature on quartz grains from aeolian and glacial environments (Costa et al., 2013; Mahaney, 2002). Previous studies also postulated that quartz abrading mechanisms in wind or sandstorm collisions can cause upturned plates (Krinsley and Wellendorf, 1980). Bulbous edges are prominent projecting and rounded grain edges in a parabolic curve (Mahaney, 2002; Vos et al., 2014). The highest percentage of bulbous edges has been observed in Unit 5 (SAK645, 64 %) bulbous edges features defined by Mahaney (2002) as prominent, protruding, and rounded grain edges. Costa et al. (2013) conducted an experimental study that proved that bulbous edges often occur with smoother-over or polished elongated depressions and are often considered the hallmark of aeolian transport. Whereas rounded edges and protrusions result from saltating grains rotating, a rare microtexture in grains under 150 μm indicates an aeolian transit phase (Mahaney, 2002). The highest percentage (40 %) of adhering particles (AP) has been observed throughout the Unit 4 (SAK405 sample); this AP can provide information of rock source areas or diagenetic environments. In most cases, nanometer-scale adhering particles, covering up to 10 % of the grain surface, are characteristic of glacial and certainly aeolian environments (Mahaney, 2002; Vos et al., 2014).

Compared to the Phase-2, the dominant microstructural features observed in Phase-1 are large conchoidal fractures (F) and angular to subangular shapes on quartz grains, which are attributed to the process of river transportation. The interaction between quartz grains and pebbles or gravel can lead to the development of larger conchoidal (>50 μm) cracks (Mahaney, 2002; Reddad et al., 2016). In chemical weathering, the solution pits (SP) show the highest median value, whereas silica pellicle (SIP) show the lowest values. Interestingly, in the case of both the features, arcuate/circular/polygonal cracks (ACPC) represent the high-

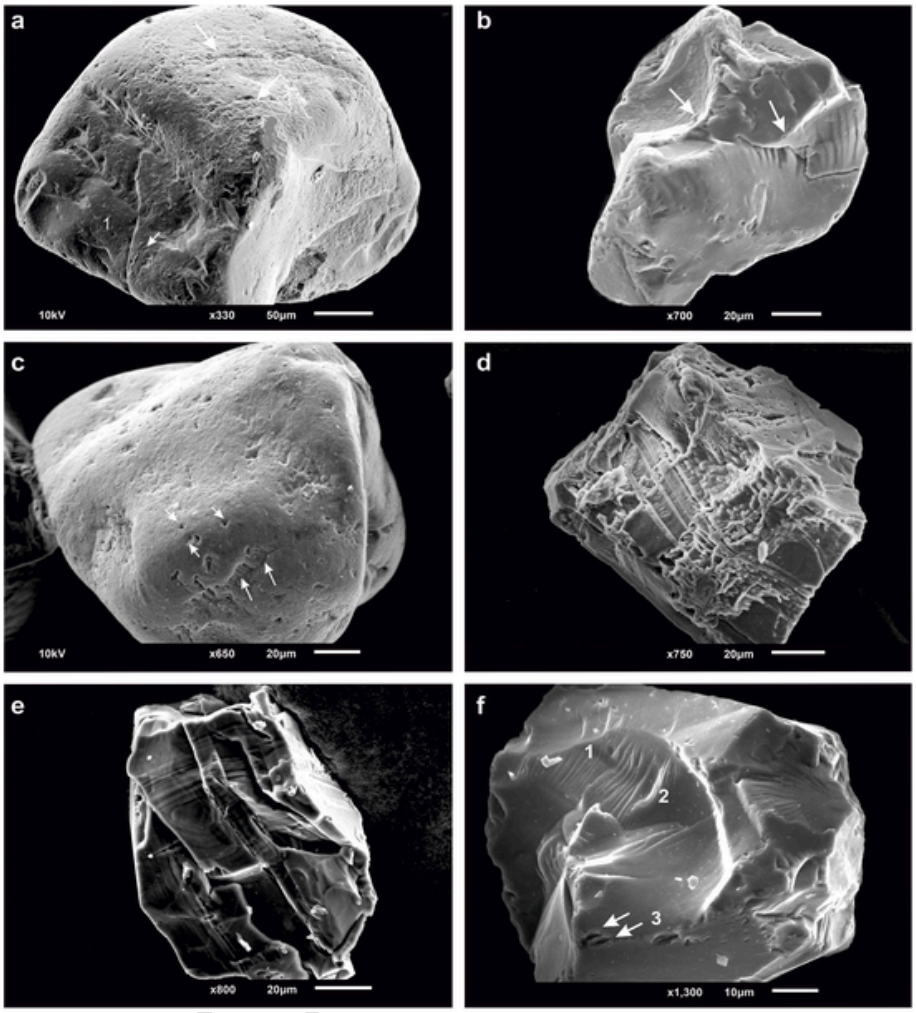

Fig. 6. From Phase 1 sediment package (Unit 1 and 2) showing (a) The SEM image of quartz grain showing the sub-rounded pattern with low to medium relief, clear expressions of straight and curved grooves and scratches (arrows); contains V-shape percussion cracks on the surface (1). (b) Small (>10 μm) and medium (> 50 μm) conchoidal fracture with arcuate steps (c) Showing well-rounded grain with a thick amorphous precipitation layer with "raindrop" structures, different type of eatch pits (arrow; rounded, triangular), the presence of extremely regular etch triangles on crystal planes suggests that the atomic structure of the crystal strongly controls the etching process. Each plane likely presents a different atomic arrangement to the etchant, leading to the formation of distinct but consistently shaped etch patterns; (d) Grain showing contains adhered particles with crystal overgrowth features (e) Angular grain with sharp edges and fresh surface features of grain, (f) Conchoidal fracture (>50 μm) has been observed below the fresh fracture; 1. some adhering particles are also present; 2. the straight, meandering and steps are present on the fracture plane; 3. typical irregular outline (>1 μm) and various sizes of triangular etch pits are presents.

est median value (~38), and chattermarks (CM) represent the lowest value. The V-shaped percussion cracks were not found in Phase-2 but were found in medium coarse quartz grains samples of SAK001, SAK085, SAK165 (10.2, 6.67, 9.3 %, respectively) from Phase 1 sediment package. Vos et al. (2014) confirmed that the pits are probably the results of weathering in marine and aeolian environments, whereas, Křížek et al. (2017) identified pits are formed in glacio-fluvial environments. The abundance of oriented etch pits and pitting on grains varied, especially at the start of fluvial transport, due to diurnal and annual discharge fluctuations during high stream power and more frequent channel changes in braided rivers (Kane and Yang, 2004), due to which alkaline solutions can slowly etch the sediments in a non-aquatic setting (Doornkamp and Krinsley, 1971).

Based on the identification of the results, more common surface textures observed in the quartz grains are represented by meandering ridges, straight/curved grooves, and scratches, abrasion fatigue, oriented etch and solution pits with low relief, elongated depressions and arcuate cracks respectively. The conchoidal fracture (<10 μm) in the complex silty-clay samples (Unit 4 and 5; SAK405 and SAK645) accounted for 41 % and 37.46 %. The conchoidal fractures are shell-shaped breakage patterns with prominent arc forms and overlapping (Vos et al., 2014; Wu et al., 2020). This study observed arcuate and straight steps in the refined grains fraction of Phase-2 package samples, in proportion range varying from 11 to 21 % and 17–24.77 %, respectively. The least common texture was scaling, chattermarks, and large conchoidal fracture (>100 μm), which occurred on <5 % of the grains. The V-shaped percussion cracks, triangular depressions, and shallowly indented depressions are evidence of mechanical impacts (Vos et al., 2014). The box plot diagram (Fig. 9) showing the subangular outline (SO) feature represents the highest frequency number in mechanical weathering feature, where large conchoidal fracture (LCF; > 100 μm) represents the lowest frequency.

4.3. Principal component analysis (PCA)

The PCA graphs displays (Fig. 10) the positioning of each sediment sample regarding identified components. These PCA had the capacity to explain a total of 86.5 % of the variance in the first data (all textures),

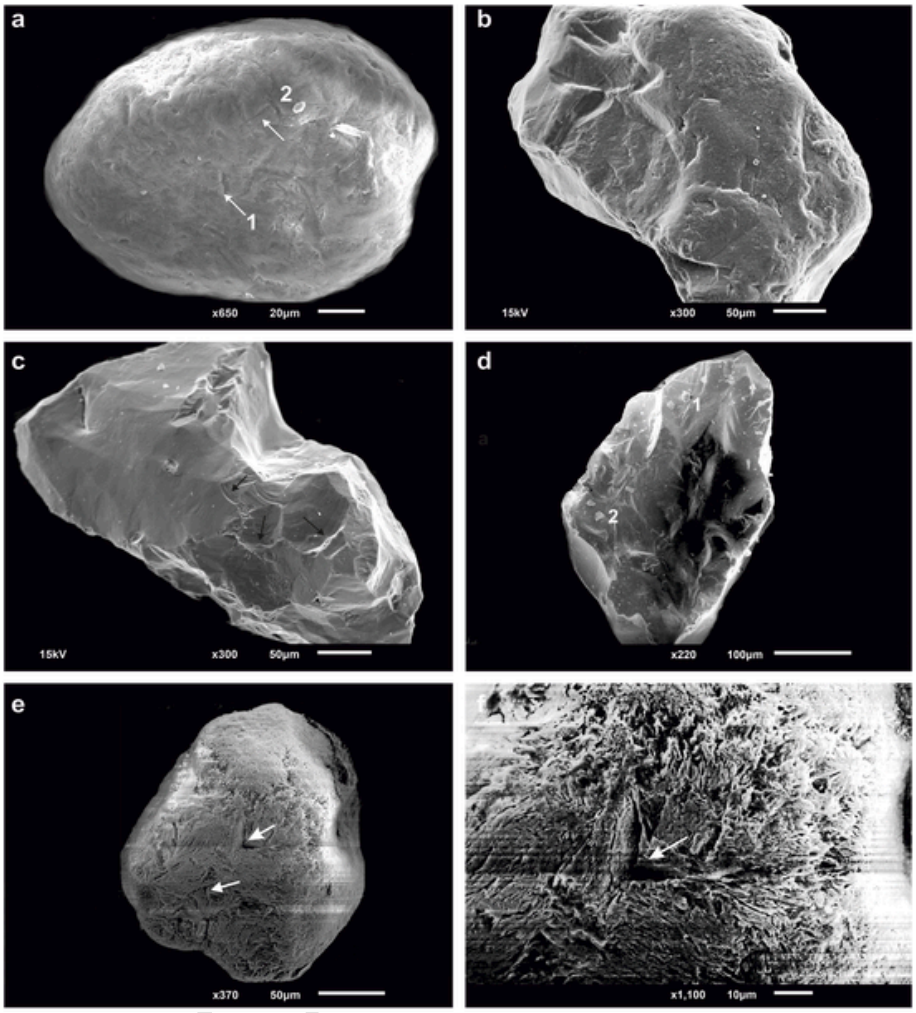

Fig. 7. The SEM images of (a) Quartz grain of sample with rounded outline and low relief; (arrows), 1. solution pits and crevasses are much prominent, 2. some adhering particles are present on the surface. (b) Sub-angular grain is moderately altered (in this case, bulbous edges, fractures and steps). (c) Quartz grain representing conchoidal fractures (>20–40 μm) with high fluvial energy condition, sharp edges, a fracture plane with the clear presence of numerous chattermarks, widened by solution. (d) Angular grain with sharp edges and medium to large conchoidal (<100 μm) fractures, 1 and 2 are medium flakes probably originating from another grain are adhering on the surface (top and bottom) (e) A grain covered by precipitation, crescentic marks (f) Enlargement of grain V–shaped percussion crack (arrow) developed on the grain surface.

with the top three PCA having the ability to explain 78.08 % of the variance (Table 5) and a total of 90.2 % of the variance in the second data (mechanical) with the top three PCA having the ability to explain 83.86 % of the variance.

4.3.1. PCA: all texture parameter

The PC1 of all texture parameters has the highest variance of 37.66 % with strong positive loadings imparted by crescentic percussion marks, silica flowers, V–shaped percussion cracks, arcuate/circular/polygonal cracks, chattermarks and small conchoidal fractures (<10 μm). In this case, crescentic percussion marks (CPM) and V–shaped percussion cracks (VSPC) showed the highest positive loading value for PC1, suggesting they tend to occur together when mechanical weathering occurs. SF, ACPC and CM followed closely behind. The PC1 is governed by mechanical weathering, showing that the CPM and VSPC predominantly mediated during monsoon time. The most significant negative values in PC1 represent the, SA, AF and IGF group. BE. and SCF made up the highest negative loadings for PC2; on the other hand, MCF and SIP made up the highest negative loadings for PC3. When the PC1, PC2 and PC3 (x, y and z axes, respectively; Fig. 10) shows that the majority of the SAK samples plot in the positive x and y quadrant, it corresponds to high amounts of arcuate/circular/polygonal cracks and straight/curved grooves and scratches. On the other side of the sample distribution, the section exhibits the most significant spread of any of the locations, ranging from highly positive PC2 loadings to extremely negative PC2 loading values. In this case, most of the sample distribution represents the negative values except SAK645 and SAK485 (Unit 4, 5; Fig. 10b–d) of Phase-2 package sediment cycle.

4.3.2. PCA: mechanical textures

In this case, only the mechanical textures were evaluated in the second PCA test, and the first three components here captured more than 83 % of the total variation in the data (Table 5). PC1 received the most positive loading from the occurrence of crescentic percussion marks (CPM), followed by V–shaped percussion cracks (VSPC) and small conchoidal fractures (<10 μm; SCF) features, and the most negative loading from the occurrence of abrasion fatigue (AF) and imbricated grinding features (IGF). Both straight upturned plates (UP) and straight steps (SS) showed significantly the highest positive loading values for PC2, while bulbous edges (BE) had the highest negative loading values, re-

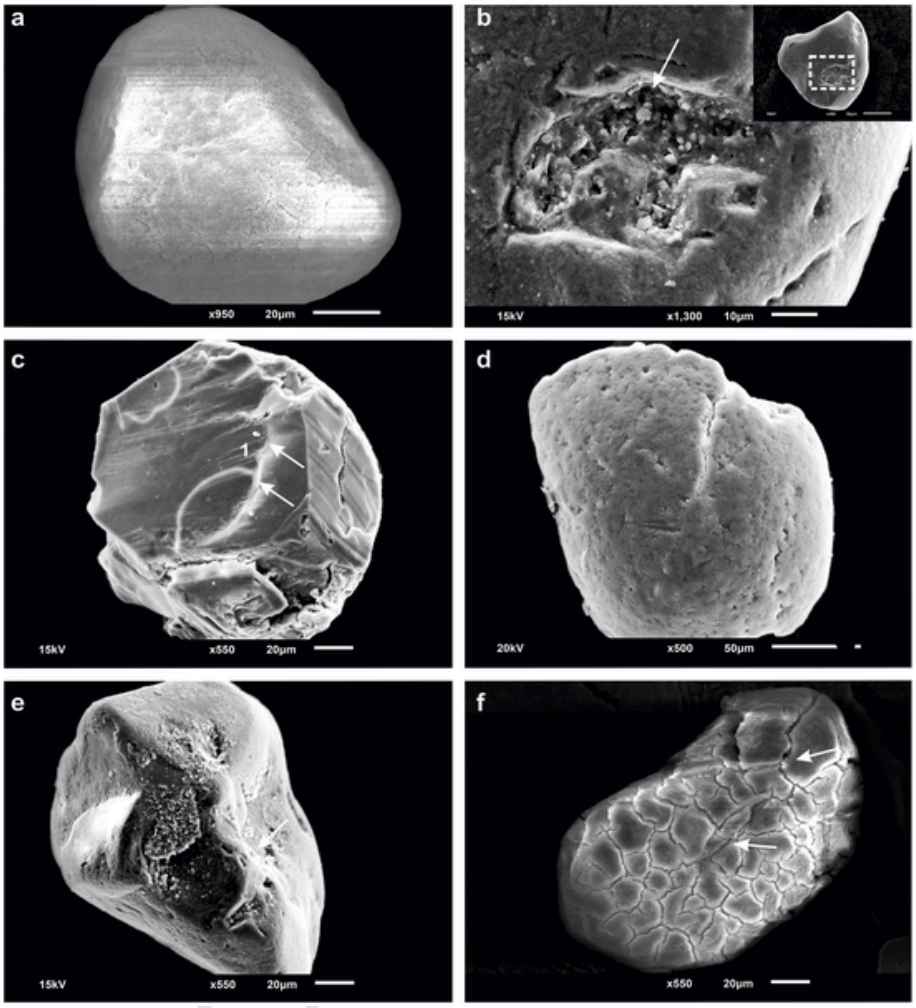

Fig. 8. From Phase 2 sediment package (Unit 4 and 5) SEM images of quartz grains showing (a) The rounded quartz grain with bulbous edges; surface has been changed by dissolution; there are present of crescent-shaped lines and amorphous precipitation layer (b) Detail of dissolution, triangular etches pits and solution pits. (c) Slow silica precipitation (down side) can form crystalline overgrowth clear with numerous chattermark which may be widened through solution. (d) Oriented etch (1–10 µm) pits and triangular v-shaped percussion cracks are also presents on the sub-rounded grain, desiccation cracks are formed due to weathering. (e) Sub-rounded with bulbous edges meandering ridge, small pits, large groove (opposite to the arrow point) fracture. (f) Quartz grain showing many cracks fracture on surface plane represent high-medium energy condition and with straight long grooves (right side).

spectively. For more details of the loading values, see Table 6, and for associations between microtextures and principal components (see Fig. 10c). Fig. 10d shows the data projected onto PC1 and PC2, where the SAK485 sample shows the highest positive values, and SAK645 sample shows the highest negative values. It indicates that the SAK485 (Unit 4) sample is essentially influenced by CPM, UP, and VSPC features.

5. Discussion

5.1. Distinct depositional phases: sedimentological and magnetic susceptibility insights

The statistical parameters derived from GSD effectively distinguish two different depositional phases. The uniformity and low-energy conditions observed in Phase-2 require further investigation. A substantial increase in energy conditions, indicated by the increase in mean grain size from Phase-2 to Phase-1, suggests a significant shift in the environmental setup (Folk and Ward, 1957). Given fluvial terrace sediments respond variably to local and global climate shifts (Schanz et al., 2018), this study does not attempt to correlate the observed stratigraphic sequence (from Phase-1 to Phase-2) to specific climate events. Instead, the focus remains on deciphering the sedimentological processes governing the environment of deposition.

Magnetic susceptibility data supports depositional phase differentiation. Unit 3 exhibits higher average χ_{lf} values ($> 3900 \times 10^{-8}$ m^3 kg^{-1}), suggesting increased sediment flux, possibly linked to enhanced hydroclimatic conditions and fluvial processes. A notable gradual decrease in χ_{lf} values ($\sim 600 \times 10^{-8}$ m^3 kg^{-1}) is observed in Units 4 and 5, indicating reduced sediment supply under weak hydroclimatic conditions.

The frequency dependent susceptibility values (χ_{fd} and $\chi_{fd\%}$) are influenced by both the GSD and the concentration of particles close to the SP/SD threshold (Eyre, 1997; Liu et al., 2005). A low $\chi_{fd\%}$ (< 15 %) indicates low SP particle levels, a wide GSD, or a bimodal GSD, while values < 5 % suggest very fine ferrimagnetic grains (~ 0.02 µm). The $\chi_{fd\%}$ value confirms variations in SP particle concentration across the unit. A consistently low $\chi_{fd\%}$ values suggest that the magnetic signal is more likely dominated by detrital inputs (Dearing et al., 1996), possibly derived from enhanced erosion and sediment transport during periods of stronger monsoon activity. A minor pedogenic contribution cannot be ruled out—particularly under wetter conditions favorable for soil formation—but its influence is considered minimal and is interpreted with

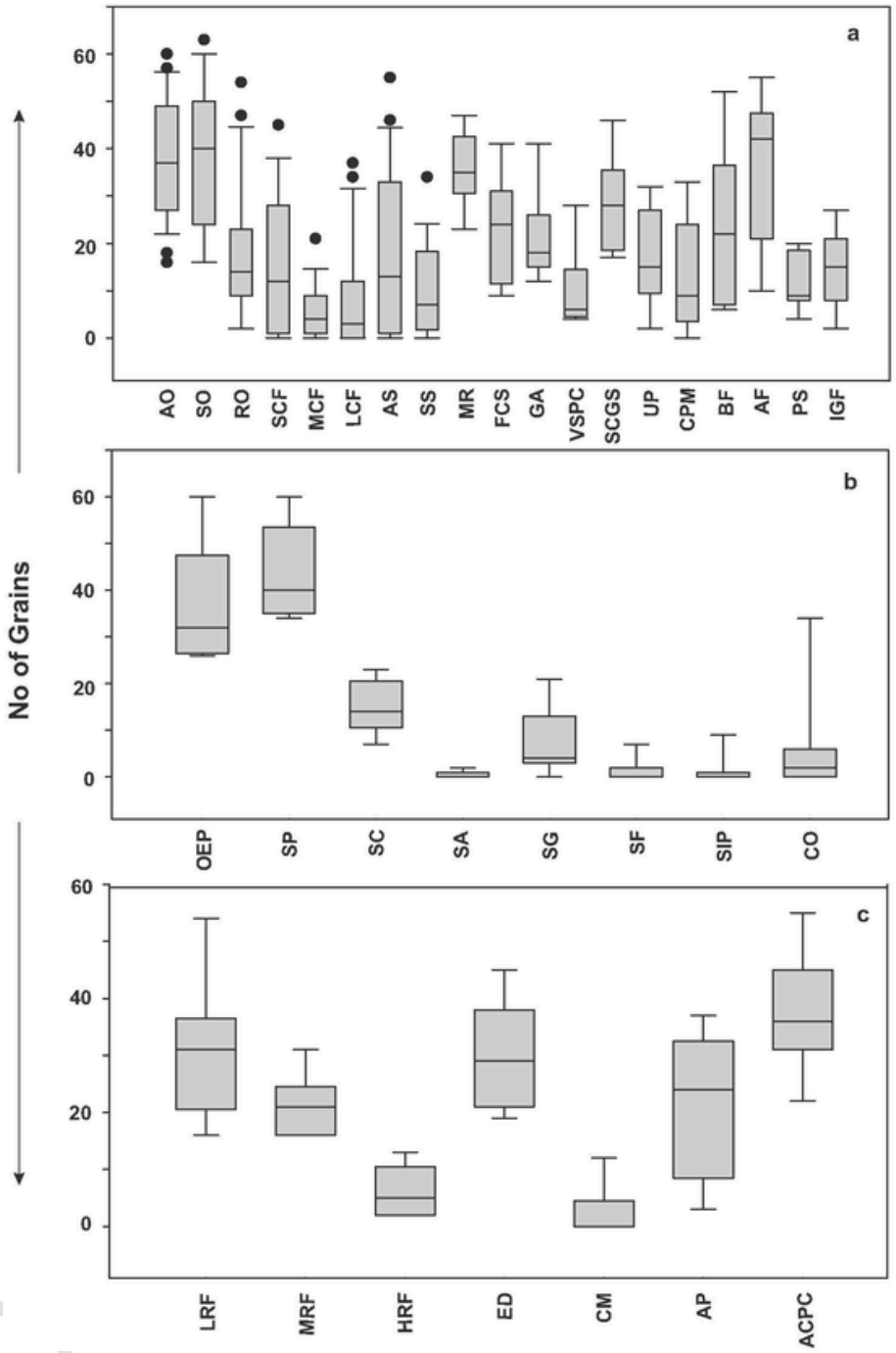

Fig. 9. Box plots represent the (a) Mechanical, (b) Chemical and (c) Mechanical and Chemical both features (the black dots represents outliers).

caution. A strong linear correlation between χ_{lf} and χ_{fd} observed in Unit 2 (R2 = 0.66), Unit 3 (R2 = 0.43), and Unit 5 (R2 = 0.52) suggests the influence of SD particles. In contrast, Unit 1 (R2 = 0.12) and Unit 4 (R2 = 0.01) indicates variable SD to SP grain concentration. These differences highlight the varying degrees of pedogenic alteration and detrital input between the units.

5.2. Fluvial microtextures and depositional processes from Phase-1 sediment package

The formation of Quaternary landforms in the middle and lower reaches of the Tapi valley, which are solely supplied with sand from local rivers, presents a valuable prospect for comprehensively observing alterations in texture and mineral composition during the transition from fluvial to aeolian processes or via versa. Additionally, the magnetic enhancement in channel and floodplain facies reflects different processes. The SAK section magnetic data (Fig. 3) show a sharp peak in χ_{lf} values at 5.1 & 5.5 m, which suggesting high detrital influx of ferromagnetic minerals. So, this Phase-1 sediment are inferred to represent a response might be a transition from early Holocene warm-humid conditions with higher precipitation and high sediment yield.

The above mentioned micro-structure results from Phase-1 sediment package (Units 1, 2 and 3), which are mostly dominated in abundant angular to subangular quartz grains with bulbous edges, solution pits,

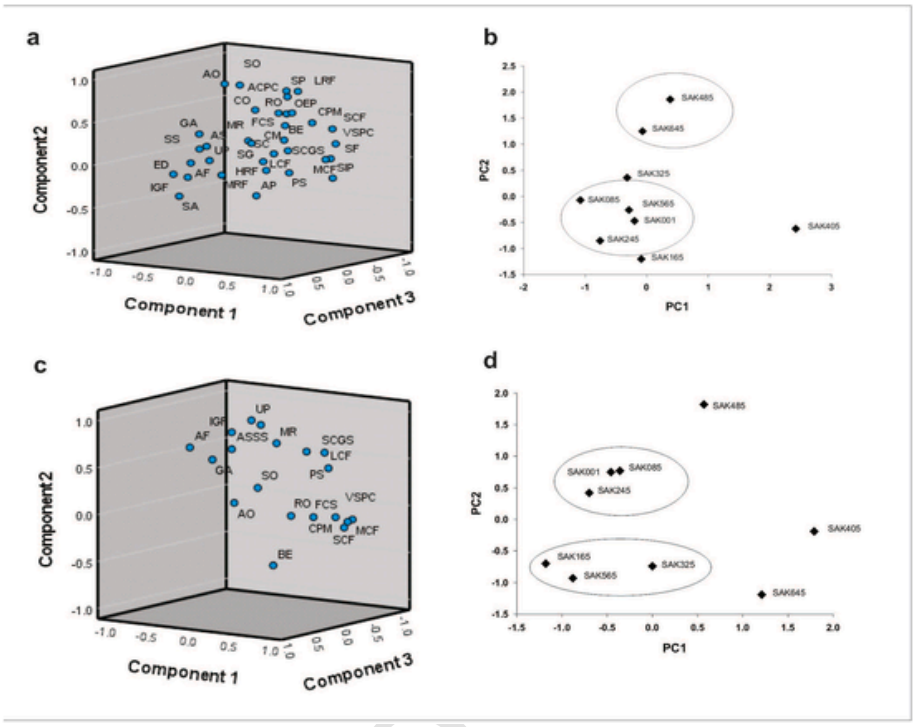

Fig. 10. Plots from principal component analysis (PCA), (a) Scatter plot of all textures variables projected onto PC1, PC2 and PC3. (b) Scatter plot of site intra-sample plotted onto projections of all textures PC1 and PC2. (c) Scatter plot of only mechanical textures variables projected onto PC1, PC2 and PC3. (d) Scatter plot of site intra-sample plotted onto projections of mechanical textures PC1 and PC2. See text for detailed explanation. See Table 6 for details of the microtexture abbreviations.

Table 5
The table represent the Eigen values and the variation (%) of PCA analysis for all surface features and mechanical data set.

Eigen values and variance for both Principal component analysis				
Data set	Component	Eigen value	Variation (%)	Cumulative variation (%)
All textures	PC 1	12.807	37.667	37.667
	PC 2	8.979	26.410	64.077
	PC 3	4.764	14.013	78.089
	PC 4	2.888	8.495	86.585
Mechanical	PC1	7.104	37.389	37.389
	PC 2	5.395	28.395	65.784
	PC 3	3.436	18.083	83.866
	PC 4	1.212	6.378	90.244

and elongated depressions. Also, the most common features are meandering ridges, low relief, solution pits, abrasion fatigue, and v-shaped percussion cracks, where silica globules, solution crevasses, large conchoidal fracture (>100 μm) chattermarks features such as solution pits and crevasses occur sparsely. Angular to subangular quartz grains are frequently observed in fluvial and intertidal regions, as well as in highly dynamic sub-aqueous environments such as foreshore or backshore areas (Kasper-Zubillaga et al., 2005; Krinsley and Donahue, 1968; Mahaney, 2002; Mahaney et al., 2001; Smith et al., 2018; Vos et al., 2014). The findings of this study reveal the presence of numerous medium to large conchoidal fractures and angular to subangular shapes on quartz grains, which are attributed to the process of river transportation. The interaction between quartz grains and pebbles or gravel can lead to the development of larger conchoidal (>50 μm) cracks (Mahaney, 2002; Reddad et al., 2016). The presence of quartz grains exhibiting straight and curved grooves, oriented etch deep pits, high relief, and crescentic gouges can occur because of constant high shear stress processes (Mahaney, 2002; Sweet and Soreghan, 2010; Szerakowska et al., 2018; Vos et al., 2014). However, V-shaped percussion cracks with evident straight and curved scratches were abundant in littoral, high energetic fluvial and deltaic grains (Mahaney, 2002; Mahaney et al., 2001; Smith et al., 2018) transportation from the high relief zone.

5.3. Aeolian microtextures and depositional processes from Phase-2 sediment package

The study identified from the Phase-2 sediment package standard microtextural imprints such as bulbous edges, rounded grains, adhering particles, elongated depressions, dissolution features, and abrasion marks and further prominent meandering ridges present at the basal part (Unit 4 and 5; SAK405, SAK485 and SAK645). The aeolian surface processes like coastal and desert dune sands generate meandering ridges when grains to grain collision occurs (Mejía-Ledezma et al., 2020; Silpa et al., 2016). This study characterised the microstructural characteristics of dune grains, confirming previous research by Nieter and Krinsley (1976), Lindé and Mycielska-Dowgiałło (1980), Pye and Tsoar (2009), Mahaney (2002), Costa et al. (2013) and Vos et al. (2014). Krinsley and Donahue (1968) reported five types of microtextural features characteristic of aeolian quartz grains from modern deserts, i.e., rounding of edges, upturned plates, equidimensional or elongated depressions, smooth surface, and arcuate or polygonal fracture. Another prominent feature, upturned plates on quartz grain, was observed in SAK485 samples (49 %; Unit 4) grains. Mahaney (2002) and Costa et al. (2013) reported that upturned plates are a prominent feature on quartz grains from aeolian and glacial environments. Krinsley and Wellendorf (1980) suggested quartz abraded mechanisms in wind machines or sand storm collisions can cause upturned plates. Mahaney (2002) defines bulbous edges as prominent projecting and rounded grain edges in a parabolic curve (see Vos et al., 2014). Round

Table 6
Table showcasing loading values resulting from PCA analysis of both overall surface features and mechanical microtexture features.

			All type		Mechanical	
Sr. No	Microstructure	Abbreviation	PCA-1	PCA-2	PCA-1	PCA-2
1	Crescentic percussion marks	CPM	0.906	−0.384	0.998	−0.32
2	Silica flowers	SF	0.859	−0.112		
3	V–shaped percussion cracks	VSPC	0.853	−0.392	0.933	−0.281
4	Arcuate/circular/polygonal cracks	ACPC	0.845	0.51		
5	Chattermarks	CM	0.840	0.393		
6	Small conchoidal fractures (<10 μm)	SCF	0.832	−0.448	0.921	−0.129
7	Flat cleavage surfaces	FCS	0.774	−0.349	0.894	−0.31
8	Oriented etch pits	OEP	0.757	−0.315		
9	Medium conchoidal fractures (<100 μm)	MCF	0.752	−0.300	0.838	−0.294
10	Straight/curved grooves and scratches	SCGS	0.736	0.413	0.468	0.579
11	Low relief	LRF	0.720	−0.117		
12	Silica pellicle	SIP	0.706	−0.246		
13	Rounded outline	RO	0.706	−0.367	0.787	−0.383
14	Solution pits	SP	0.678	−0.373		
15	Large conchoidal fracture (>100 μm)	LCF	0.672	0.293	0.565	0.434
16	Meandering ridges	MR	0.643	0.505	0.356	0.765
17	High relief	HRF	0.615	0.594		
18	Parallel striations	PS	0.579	0.449	0.297	0.582
19	Crystalline overgrowths	CO	0.577	0.491		
20	Imbricated grinding features	IGF	−0.104	0.921	−0.450	0.746
21	Upturned plates	UP	0.313	0.900	0.421	0.939
22	Elongated depressions	ED	−0.31	0.863		
23	Abrasion fatigue	AF	−0.373	0.804	−0.726	0.604
24	Straight steps	SS	0.426	0.782	0.119	0.927
25	Bulbous edges	BE	0.272	−0.743	0.605	−0.451
26	Silica globules	SG	0.667	0.670		
27	Adhering particles	AP	0.441	0.663		
28	Medium relief	MRF	0.354	0.590		
29	Scaling	SA	−0.410	0.523		
30	Angular outline	AO	0.307	0.68	0.304	0.219
31	Subangular outline	SO	0.593	0.66	0.532	0.391
32	Graded arcs	GA	0.166	0.437	0.231	0.636
33	Solution crevasses	SC	0.565	−0.329		
34	Arcuate steps	AS	0.109	0.557	−0.145	0.659

edges and protrusions result from saltating grains rotating, a rare microstructure in grains under 150 μm (Mahaney, 2002). Thus, bulbous edges indicate aeolian transit phases. The experiment proved that bulbous edges often occur with smoother-over or polished elongated depressions, often considered the hallmark of aeolian transport (Costa et al., 2013).

Two sedimentary cycles (Phase-1 and 2; Fig. 3) are comparable to those in the Sakegaon section. The basal Unit comprises aeolian yellowish silt pockets with minor clay mottling; it lacks calcrete and is stratified. The mean size representing medium to fine silt deposits (Units 4 of SAK section) and sandy-gravel Unit 3 overlying by Unit 4 is assigned to the increasing hydraulic low energy to high energy conditions. Based on the different microstructural features of quartz grains described above, it was found that the quartz grains in hard silty-clay layer (Phase-2) had been through long-term supergene geological processes before they accumulated. This first cycle of sedimentation, showing the high χ_{lf} with correspondingly low χ_{fd}, indicates detrital influx of magnetic minerals associated with silts, whereas, few peaks of χ_{lf} indicate magnetic enhancement due to pedogenic activity (Dearing et al., 1996). In the Phase-2, reduced flux of bulk magnetic minerals (e.g., χ_{lf}) suggested that a weak Indian Summer Monsoon (ISM) intensity prevailed in the region during this period of time. However, due to the provisional lack of a chronological framework from the studied section, we are not in a position to provide detailed interpretation of those hard silty-clay depositional age and sedimentation rate in the basin's geomorphic reaction to Late Quaternary climatic change. In additional features of the dune grain pattern, i.e., elongated depressions, adhering particles and rounded outlines, are formed by physical and chemical processes (Vos et al., 2014). The maximum amount of quartz grains with adhering particles from SAK section are observed in Unit 4 and 5 (SAK405, and SAK485 samples). According to Mahaney (2002), these adhering particles refer to fragments or particles clinging to the grains, such as quartz grains originating from source rocks or diagenetic settings. On the other side, the formation of the elongated depression is attributed to a high-energetic aeolian transport situation, and it is often smoothed over by silica precipitation between upturned plates (Vos et al., 2014).

5.4. Regional significance

Loess deposits are widely distributed in the Indian subcontinent on mountain slopes and river terraces (Bhattacharya et al., 2017; Liu et al., 2017; Sinha et al., 2007a). Loess deposition (Phase-2 sediment package) at SAK section in the Tapi valley offers a unique opportunity to study textural and mineralogical changes during the fluvial-aeolian transition. Given the proximity of the study location to the TD (as illustrated in Fig. 1a), which is already established as a primary dust source in north-western and central India (Liu et al., 2017; Sinha et al., 2009; Yadav et al., 2007), the section holds significant potential for further investigation into understanding continental responses to changing monsoon dynamics. Singhvi and Kar (2004) note that sand and dust-raising winds begin in western India from March onwards when the surface is dry and the maximum wind speed of 20 km/h or more during June. The deposition of the dust and silt in Phase-2 package of the SAK base section on the Tapi river bank shows the deposition is characterized by relatively medium grain size (3.5–6.6 ϕ), poor sorting, and highly negative skewness, reflecting a short-distance transport by deflation of loose fluvial and aeolian deposits nearby. But grain roundness (0.3–0.4) increases at the transition from the fluvial to the aeolian environment formed at a greater distance. According to Wang et al. (2017), the mi-

crotextures on quartz surfaces can be used as "fingerprints" to trace the provenance of sediment through a comprehensive comparison with potential sources. It was observed that the Sakegaon quartz grains in the hard silty-clay layer (Unit 4) had experienced very long-term supergene geologic processes before they were deposited with the Phase-2 sediment package. This was shown to be the case after analyzing the numerous microtextural features of quartz grains, which were discussed above. Similarly, the cluster analysis results of groups and similarities of different parameter are shown in the dendrogram (Supplementary Fig. S5). Further, the dendrogram illustrates two primary groups, delineated as package Phase-1 and Phase-2. The first group (comprising Unit 1, 2, and 3) encompasses the majority of samples, indicative of a predominantly fluvial-dominated process. Within this group, two subgroups are discernible, each associated with fluvial sand characteristics. In contrast, the second group (consisting of Unit 4 and 5) includes samples such as SAK405 and SAK645, demonstrating a significant correlation with aeolian sand properties and other geomorphic processes.

In summary, the properties of quartz grains within the Phase-2 sediment package suggest an aeolian origin. Two distinct scenarios are proposed: (1) direct wind transportation of dust from its source to the deposition area, or (2) initial transportation of materials by fluvial processes into the sedimentary system, followed by subsequent wind-driven accumulation. To better understand such changes, a more comprehensive dataset of past climate, provenance indicators and chronologies is necessary.

Past climatic records from this region provide further insights. Two ostrich egg shell (OES) specimens were reported in surface context from the Sakegaon Quaternary sediment (Sukumaran et al., 2023a, 2023b). Both specimens are dated to 47145 ± 2180 Calibrated years BP and 53200 ± 1200 calibrated years BP, respectively. The latter specimen (53200 ± 1200 calibrated years BP) also has a $\delta^{18}O_{OES}$ value of 4.27 ‰ (VPDB), which indicates an extremely arid phase. Other sites of OES distribution are present at Katoati, Rajasthan (~35–59 ka, Blinkhorn et al., 2015), Mehtakheri (>41 ka; Mishra, 1995) and Morpani (~49 ka; Chauhan et al., 2017) in the Narmada basin during MIS 3, which clearly indicates that during this period of time, C_4 vegetation extended to other part of India (Blinkhorn et al., 2015). Similar observations were made from the Thar Desert (Jain and Tandon, 2003) and the Deccan River basin (Kale and Rajaguru, 1987) records. Herzschuh (2006) suggested the optimal moisture conditions occurred between ~43 and 37.6 ka, with a weakening after 25.5 ka and a minimum between 21.3 and 19.8 ka BP. Further, Bhattacharya et al. (2017) reported that the two major channel sand bodies separated by a pedogenesis dune sand represent the youngest (~2 ka) alluvial succession along the Saraswati River (Western India) and along the Banas River, the channel sand on the river bed at a depth 1.5 m gave an age of 1 ± 0.1 ka. The fluvial record clearly represents moist climatic conditions during the Medieval Warm Period reported from Luni River (Kale et al., 2000); Sabarmati River (Sridhar et al., 2014). *G. Bulloides* increased significantly in the eastern Arabian Sea, suggesting a brief ISM rise (Gupta et al., 2003).

The regional signatures indicate that the present study area has undergone two preliminary phases of climate conditions from the mid-late Pleistocene to the Holocene. By comparing the regional hydrodynamic conditions with those of the SAK sections and their preserved cyclicality of aeolian-fluvial processes within a single section, it presents a fundamental opportunity to conduct detailed multidisciplinary research. The recent study employing Sr-Nd isotopes has shed light on the prevalence of cold or arid phases (Shukla et al., 2024), characterized by an increased proportion of aeolian dust evident in Indian Ocean core sediments. In this connection the Sakegaon section, location in particular to the central India, holds significant value in comprehending the continental response to aeolian dust under such conditions.

In the context of Late Pleistocene paleoenvironments, further investigations are warranted to test the hypothesis of dispersal of ostriches and prehistoric *H. sapiens* into the Indian Subcontinent as a mutually exclusive but incidentally synchronous due to specific conditions such as aridity (Chauhan et al., 2015). Additional observations such as the role of prehistoric *H. sapiens* (direct and/or indirect) in the extinction of more than one faunal species including the ostrich between 50 and 10 ka (see Jukar et al., 2021) and the impact on regional hippo migration/extinction events as a result of aridity needs further careful local verses regional comparative studies. This link between intermittent phases of Late Pleistocene aridity at the local (e.g. Sukumaran et al., 2023b), regional (e. g. Jha et al., 2024) and global (e.g. Fuhrmann et al., 2020) scales and associated faunal and hominin adaptations (see Li et al., 2019) needs to be better understood through specific chrono-contextual targets (Mehra and Chauhan, 2021). In these respects, the Indian Subcontinent lies between key arid zones of western and eastern parts of Asia (e. g. Field and Wroe, 2012; Nichol and Nichol, 2013; Zhou et al., 2024) and the Tapi Basin makes for an ideal paleoanthropological study area due to its proximity to key South Asian arid zones such as the Thar Desert and the Tibetan plateau; it is also in critical biogeographic proximity to the hominin and faunal dispersal routes into the western, central and peninsular India.

6. Conclusion

This study examines sediment characteristics in the Tapi River Valley to distinguish between autochthonous and allochthonous sources of aeolian sands and defining sediment textural and compositional changes throughout the fluvial-aeolian transition. By employing a detailed quantitative analysis, the research identified microtextural features indicative of different depositional environments. The quartz micromorphology characteristics of the Phase 2 package yielded valuable insights into the aeolian history associated with this particular hard silty-clay formation. Grain size distributions indicate a single provenance for the silt grains, with magnetic data suggesting that increased bulk magnetic concentrations in Phase-1 sediment package show that more flux from catchment soil happened because of faster erosion probably due to intensified ISM and weak monsoon strength characterized by low magnetic flux in Phase-2 sediment package zone. Aerodynamic principles, roundness, and microtextures analysis reveal that fine aeolian silty material originates predominantly from proximal source regions within the middle Tapi River Basin. Overall, our research results underscore the potential impacts changing environments may have had on various faunal and human populations during the Late Pleistocene of west-central India. Further research into these areas is crucial for a more comprehensive understanding of the interplay between dust fluxes and climate, and for improving climate models.

CRediT authorship contribution statement

Sourav Mukhopadhyay: Writing – original draft, Formal analysis, Data curation. **Pratik Pandey:** Writing – review & editing, Formal analysis, Data curation, Conceptualization. **Prabhin Sukumaran:** Writing – review & editing, Writing – original draft, Supervision, Methodology, Conceptualization. **Binita Phartiyal:** Writing – review & editing, Formal analysis, Data curation. **Swati Verma:** Writing – review & editing, Formal analysis, Data curation. **Varun Vyas:** Writing – review & editing, Data curation. **Navashni Naidoo:** Writing – review & editing, Formal analysis, Data curation. **Avantika Binani:** Writing – review & editing, Formal analysis. **Jessica L. Conroy:** Writing – review & editing, Resources, Formal analysis, Data curation. **Parth R. Chauhan:** Writing – review & editing, Formal analysis, Data curation, Conceptualization.

Data availability

All relevant data used in this paper are available from the authors. Sediment samples and SEM images are held in the Charusat University, India, and in the IISER Mohali, India.

Declaration of competing interest

The authors declare that they have no known competing financial interests or personal relationships that could have appeared to influence the work reported in this paper.

Acknowledgement

This paper is a part of a collaborative research project between CHARUSAT and IISER Mohali. The work received partial financial support from the Ministry of Education (Government of India) project (STARS 651 with PRC as P.I.), a Fulbright fellowship (2666/F-N APE/2021), and the CHARUSAT Seed Research Grant to P.S. S.M. acknowledges the post-doctoral fellowship from Charusat University, India for supporting this work. S.M. and P.P. acknowledge Vanaraj Solanki (Charusat University) for training and assistance with SEM analyses. The Paleomagnetism Laboratory of Birbal Sahni Insitute of Palaeosciences, Lucknow, is acknowledged for the MS analysis. We sincerely thank all local organizations and individuals who assisted in conducting high-resolution sampling for the Tapi Valley project. P.S. acknowledges the laboratory support extended by Stanley H. Ambrose for basic sample processing for GSD.

We are also grateful to the anonymous reviewers for their valuable comments and constructive feedback, which significantly improved the logical clarity and overall quality of the manuscript. Finally, we thank our respective institutions for their continued support.

Appendix A. Supplementary data

Supplementary data to this article can be found online at https://doi.org/10.1016/j.quaint.2025.109878.

References

Bhattacharya, F., Shukla, A.D., Patel, R., Rastogi, B., Juyal, N., 2017. Sedimentology, geochemistry and OSL dating of the alluvial succession in the northern Gujarat alluvial plain (western India)-A record to evaluate the sensitivity of a semiarid fluvial system to the climatic and tectonic forcing since the late Marine Isotopic Stage 3. Geomorphology 297, 1–19.

Blinkhorn, J., Achyuthan, H., Ditchfield, P., Petraglia, M., 2017. Palaeoenvironmental dynamics and palaeolithic occupation at Katoati, Thar Desert, India. Quat. Res. 87, 298–313.

Blinkhorn, J., Achyuthan, H., Jaiswal, M., Singh, A.K., 2020. The first dated evidence for Middle-Late Pleistocene fluvial activity in the central Thar Desert. Quat. Sci. Rev. 250.

Blinkhorn, J., Achyuthan, H., Petraglia, M.D., 2015. Ostrich expansion into India during the Late Pleistocene: implications for continental dispersal corridors. Palaeogeogr. Palaeoclimatol. Palaeoecol. 417, 80–90.

Blott, S.J., Pye, K., 2001. Gradistat: a grain size distribution and statistics package for the analysis of unconsolidated sediments. Earth Surf. Process. Landf. 26, 1237–1248.

Cardona, J.M., Mas, J.G., Bellón, A.S., Domínguez-Bella, S., López, J.M., 2005. Surface textures of heavy-mineral grains: a new contribution to provenance studies. Sediment. Geol. 174, 223–235.

Chamyal, L.S., Maurya, D.M., Bhandari, S., Raj, R., 2002. Late Quaternary geomorphic evolution of the lower Narmada valley, Western India: implications for neotectonic activity along the Narmada-Son Fault. Geomorphology 46, 177–202.

Chauhan, N., Morthekai, P., 2017. Chronology of desert margin in western India using improved luminescence dating protocols. J. Earth Syst. Sci. 126, 115.

Chauhan, P.R., Krishnan, K., Tiwari, N., Mukherjee, A., Anoop, A., Sant, D.A., Patnaik, R., 2017. At the forest edge: general observations on new microlithic occurrences in the central Narmada Basin, Madhya Pradesh. In: Deo, S.G., Baptista, A., Joglekar, J. (Eds.), RISPQS Monograph No-7: Rethinking the Past: A Tribute to Professor V. N. Misra. Indian Society for Prehistoric and Quaternary Studies Pune, pp. 65–80.

Chauhan, P.R., Ozarkar, S., Kulkarni, S.J.E., 2015. Genes, stone tools, and modern human dispersals in the center of the Old World. Asia, d.o.m.h.b.i.P. In: Y, K., M, I., T, G., H, S., A, O. (Eds.), Emergence and Diversity of Modern Human Behavior in Paleolithic Asia. Texas A&M University Press, Texas, pp. 94–113.

Chmielowska, D., Woronko, B., 2019. A source of loess-like deposits and their attendant palaeoenvironment – orava Basin, Western Carpathian Mountains, S Poland. Aeolian Res. 38, 60–76.

Costa, P., Andrade, C., Mahaney, W., Da Silva, F.M., Freire, P., Freitas, M., Janardo, C., Oliveira, M., Silva, T., Lopes, V., 2013. Aeolian microtextures in silica spheres induced in a wind tunnel experiment: comparison with aeolian quartz. Geomorphology 180, 120–129.

Dearing, J.A., Dann, R., Hay, K., Lees, J., Loveland, P., Maher, B.A., O'grady, K., 1996. Frequency-dependent susceptibility measurements of environmental materials. Geophys. J. Int. 124, 228–240.

Dennell, R., 2021. Geoarchaeology in India in the 21st Century: an Outsider's Perspective. Geological Society. Special Publications, London. 515, SP515-2020-2202.

Doornkamp, J.C., Krinsley, D., 1971. Electron microscopy applied to quartz grains from a tropical environment. Sedimentology 17, 89–101.

Evans, M.E., Heller, F., 2003. Environmental Magnetism: Principle and Applications of Enviromanetics. Academic Press.

Eyre, J.K., 1997. Frequency dependence of magnetic susceptibility for populations of single-domain grains. Geophys. J. Int. 129, 209–211.

Field, J., Wroe, S., 2012. Aridity, faunal adaptations and Australian Late Pleistocene extinctions. World Archaeol. 44, 56–74.

Folk, R.L., Ward, W.C., 1957. Brazos River bar: a study in the significance of grain size parameters. J. Sediment. Petrol. 27, 3–26.

Fuhrmann, F., Diensberg, B., Gong, X., Lohmann, G., Sirocko, F., 2020. Aridity synthesis for eight selected key regions of the global climate system during the last 60 000 years. Clim. Past 16, 2221–2238.

Groucutt, H.S., Petraglia, M.D., Bailey, G., Scerri, E.M.L., Parton, A., Clark-Balzan, L., Jennings, R.P., Lewis, L., Blinkhorn, J., Drake, N.A., Breeze, P.S., Inglis, R.H., Devès, M.H., Meredith-Williams, M., Boivin, N., Thomas, M.G., Scally, A., 2015. Rethinking the dispersal of Homo sapiens out of Africa. Evol. Anthropol. 24, 149–164.

Gupta, A.K., Anderson, D.M., Overpeck, J.T., 2003. Abrupt changes in the Asian southwest monsoon during the Holocene and their links to the North Atlantic Ocean. Nature 421, 354–357.

Herzschuh, U., 2006. Palaeo-moisture evolution in monsoonal Central Asia during the last 50,000 years. Quat. Sci. Rev. 25, 163–178.

Hu, G., Hu, J., Yu, L., Yang, L., Liu, X., Xiao, F., Dong, Z., 2023. Holocene aeolian activity triggered by climate change and endorheic-exorheic drainage transition in the Headwater Region of the Yellow River, Tibetan Plateau. Geomorphology 441, 108890.

Jain, M., Tandon, S.K., 2003. Fluvial response to Late Quaternary climate changes, western India. Quat. Sci. Rev. 22, 2223–2235.

Jha, D.K., Vaishnav, H.K., Roy, N., 2024. Late quaternary human-environment relationship in the Ganga plain, India. Quat. Int. 680, 1–16.

Jolliffe, I.T., Cadima, J., 2016. Principal component analysis: a review and recent developments. Phil. Trans. Math. Phys. Eng. Sci. 374, 20150202.

Jukar, A.M., Lyons, S.K., Wagner, P.J., Uhen, M.D., 2021. Late quaternary extinctions in the Indian subcontinent. Palaeogeogr. Palaeoclimatol. Palaeoecol. 562, 110137.

Juyal, N., Rachna, R., Maurya, D.M., Chamyal, L.S., Singhvi, A.K., 2000. Chronology of Late Pleistocene environmental changes in the lower Mahi basin, western India. J. Quat. Sci. 15, 501–508.

Kale, V.S., Rajaguru, S.N., 1987. Late Quaternary alluvial history of the northwestern Deccan upland region. Nature 325, 6–8.

Kale, V.S., Singhvi, A.K., Mishra, P.K., Banerjee, D., 2000. Sedimentary records and luminescence chronology of late Holocene palaeofloods in the Luni River, Thar Desert, northwest India. Catena 40, 337–358.

Kalińska, E., Nartišs, M., 2014. Pleistocene and Holocene aeolian sediments of different location and geological history: a new insight from rounding and frosting of quartz grains. Quat. Int. 328, 311–322.

Kane, D.L., Yang, D., 2004. Overview of water balance determinations for high latitude watersheds. IAHS Publication. Series Proc. Rep. 290, 1–12.

Kar, A., Singhvi, A.K., Rajaguru, S.N., Juyal, N., Thomas, J.V., Banerjee, D., Dhir, R.P., 2001. Reconstruction of the late quaternary environment of the lower Luni plains, Thar Desert, India. J. Quat. Sci. 16, 61–68.

Kasper-Zubillaga, J., Dickinson, W., Carranza-Edwards, A., Hornelas-Orozco, Y., 2005. Petrography of quartz grains in beach and dune sands of Northland, North Island, New Zealand. N. Z. J. Geol. Geophys. 48, 649–660.

Kemnitz, H., Lucke, B., 2019. Quartz grain surfaces–A potential microarchive for sedimentation processes and parent material identification in soils of Jordan. Catena 176, 209–226.

Krinsley, D., Wellendorf, W., 1980. Wind velocities determined from the surface textures of sand grains. Nature 283, 372–373.

Krinsley, D.H., Donahue, J., 1968. Environmental interpretation of sand grain surface textures by electron microscopy. Geol. Soc. Am. Bull. 79, 743–748.

Křížek, M., Krbcová, K., Mida, P., Hanáček, M., 2017. Micromorphological changes as an indicator of the transition from glacial to glaciofluvial quartz grains: evidence from Svalbard. Sediment. Geol. 358, 35–43.

Li, F., Vanwezer, N., Boivin, N., Gao, X., Ott, F., Petraglia, M., Roberts, P., 2019. Heading north: late Pleistocene environments and human dispersals in central and eastern Asia. PLoS One 14, e0216433.

Li, Z., Yu, X., Dong, S., Chen, Q., Zhang, C., 2020. Microtextural features on quartz grains from eolian sands in a subaqueous sedimentary environment: a case study in the hinterland of the Badain Jaran Desert, Northwest China. Aeolian Res. 43, 100573.

Lindé, K., Mycielska-Dowgiałło, E., 1980. Some experimentally produced microtextures on grain surfaces of quartz sand. Geogr. Ann. Phys. Geogr. 62, 171–184.

Liu, Q., Roberts, A.P., Larrasoaña, J.C., Banerjee, S.K., Guyodo, Y., Tauxe, L., Oldfield, F., 2012. Environmental magnetism: principles and applications. Rev. Geophys. 50, RG4002.

Liu, Q., Torrent, J., Maher, B.A., Yu, Y., Deng, C., Zhu, R., Zhao, X., 2005. Quantifying grain size distribution of pedogenic magnetic particles in Chinese loess and its

significance for pedogenesis. J. Geophys. Res. Solid Earth 110.
Liu, X., Ma, M., Wu, H., Zhou, Z., 2017. Identification of aeolian loess deposits on the Indo-Gangetic Plain (India) and their significance. Sci. China Earth Sci. 60, 428–437.
Mahaney, W.C., 2002. Atlas of Sand Grain Surface Textures and Applications. Oxford University Press, USA.
Mahaney, W.C., Stewart, A., Kalm, V., 2001. Quantification of SEM microtextures useful in sedimentary environmental discrimination. Boreas 30, 165–171.
Malik, J.N., 1996. The quaternary sedimentation and neotectonism in lower Tapi valley. Man Environ. 20, 1–9.
Marshall, J., Bull, P., Morgan, R., 2012. Energy regimes for aeolian sand grain surface textures. Sediment. Geol. 253, 17–24.
Mehra, S.B., Chauhan, P.R., 2021. Late Pleistocene environments of South Asia: a review of multidisciplinary research and relevance for understanding hominin environmental adaptations. Man Environ. 46.
Mejía-Ledezma, R., Kasper-Zubillaga, J., Alvarez-Sánchez, L., Mendieta-Lora, M., Arellano-Torres, E., Tetlalmatzi-Martínez, J., Gonzalez-Bermúdez, A., Patiño-Andrade, D., Armstrong-Altrin, J., 2020. Surface textures of quartz and ilmenite grains from dune and beach sands of the Gulf of Mexico Coast, Mexico: implications for fluvial, aeolian and marine transport. Aeolian Res. 45, 100611.
Merh, S.S., Chamyal, L.S., 1993. The Quaternary sediments in Gujarat. Curr. Sci. (Bangalore) 64, 823–827.
Mishra, S., 1995. Chronology of the Indian Stone Age: the impact of recent absolute and relative dating attempts. Man Environ. 20, 11–16.
Nichol, J.E., Nichol, D.W., 2013. Pleistocene loess in the humid subtropical forest zone of East Asia. Geophys. Res. Lett. 40, 1978–1983.
Nieter, W.M., Krinsley, D.H., 1976. The production and recognition of aeolian features on sand grains by silt abrasion. Sedimentology 23, 713–720.
Panwar, S., Yang, S., Srivastava, P., Khan, M.Y.A., Sangode, S.J., Chakrapani, G.J., 2020. Environmental magnetic characterization of the Alaknanda and Ramganga river sediments, Ganga basin, India. CATENA 190, 104529.
Pye, K., Tsoar, H., 2009. Aeolian Sand and Sand Dunes. Springer Science & Business Media.
Reddad, H., El Talibi, H., Perri, F., El Moussaoui, S., Zerdeb, M.A., Zaghloul, M.N., Critelli, S., 2016. Textural and compositional controls on modern fluvial and beach sands of Mediterranean coastal Rif belt (Northern Rif, Morocco). Italian J. Geosci. 135, 336–349.
Sali, S., 1985. The Upper Palaeolithic Culture at Patne, District Jalgaon, Maharashtra. Recent Advances in Indo-Pacific Prehistory (New Delhi 1985). pp. 137–145.
Sali, S., 1989. The Upper Palaeolithic and Mesolithic Cultures of Maharashtra. Deccan College Post-Graduate and Research Institute, Pune.
Sali, S., 1990. Quaternary environment and culture change in the central Tapi Basin. Bull. Deccan Coll. Res. Inst. 49, 375–404.
Sangode, S.J., Sinha, R., Phartiyal, B., Chauhan, O.S., Mazari, R.K., Bagati, T.N., Suresh, N., Mishra, S., Kumar, R., Bhattacharjee, P., 2007. Environmental magnetic studies on some Quaternary sediments of varied depositional settings in the Indian sub-continent. Quat. Int. 159, 102–118.
Schanz, S.A., Montgomery, D.R., Collins, B.D., Duvall, A.R., 2018. Multiple paths to straths: a review and reassessment of terrace genesis. Geomorphology 312, 12–23.
Schneider, C.A., Rasband, W.S., Eliceiri, K.W., 2012. NIH Image to ImageJ: 25 years of image analysis. Nat. Methods 9, 671–675.
Shukla, A., Singh, S.K., Singh, D.P., Sharma, A., Dimri, A.P., 2024. Strong climate control on the millennial-scale dust variability and sediment provenances in the equatorial Indian ocean inferred from Sr-Nd isotopes. Paleoceanogr. Paleoclimatol. 39, e2023PA004808.
Silpa, B., Srinivas, R., Likhil, A., Aneesh, T., Prasad, K., Sajan, K., 2016. Microtextures on quartz grains in the beach sediments of a high energy regime, Kerala, Southwest coast of India. Indian J. Geo Mar. Sc. 45.
Singhvi, A., Kar, A., 2004. The aeolian sedimentation record of the Thar Desert. J. Earth Syst. Sci. 113, 371–401.
Sinha, R., Bhattacharjee, P., Sangode, S., Gibling, M., Tandon, S., Jain, M., Godfrey-Smith, D., 2007a. Valley and interfluve sediments in the southern Ganga plains, India: exploring facies and magnetic signatures. Sediment. Geol. 201, 386–411.
Sinha, R., Bhattacharjee, P.S., Sangode, S.J., Gibling, M.R., Tandon, S.K., Jain, M., Godfrey-Smith, D., 2007b. Valley and interfluve sediments in the Southern Ganga Plains. India: exploring facies and magnetic signatures. Sediment. Geol. 201, 386–411.
Sinha, R., Kettanah, Y., Gibling, M.R., Tandon, S.K., Jain, M., Bhattacharjee, P.S., Dasgupta, A.S., Ghazanfari, P., 2009. Craton-derived alluvium as a major sediment source in the Himalayan Foreland Basin of India. GSA Bull. 121, 1596–1610.
Smith, C., Soreghan, G.S., Ohta, T., 2018. Scanning electron microscope (SEM) microtextural analysis as a paleoclimate tool for fluvial deposits: a modern test. GSA Bull. 130, 1256–1272.
Sridhar, A., Chamyal, L., Patel, M., 2014. Palaeoflood record of high-magnitude events during historical time in the Sabarmati River, Gujarat. Curr. Sci. (Bangalore) 107, 675–679.
Sukumaran, P., Ambrose, S.H., Chauhan, P.R., 2023a. Morphology, radiocarbon dating and stable isotopes analysis from eggshell of extinct ostrich from Central Tapi River Valley, India. In: Paleoanthropological Significance, XXI INQUA Congress 2023. Rome, Italy.
Sukumaran, P., Li, H.-C., Lin, J.-P., Chauhan, P.R., 2023b. Prehistoric landscapes, humans and ostriches: highlighting geoarchaeological issues in the Tapi Basin of Maharashtra (west-central India) – a multidisciplinary approach. In: Tiwari, N., Singh, V., Mehra, S.B. (Eds.), Quaternary Geoarchaeology of India. Geological Society of London, pp. 169–196.
Sweet, D.E., Soreghan, G.S., 2010. Application of quartz sand microtextural analysis to infer cold-climate weathering for the equatorial Fountain Formation (Pennsylvanian–Permian, Colorado, USA). J. Sediment. Res. 80, 666–677.
Szerakowska, S., Woronko, B., Sulewska, M.J., Oczeretko, E., 2018. Spectral method as a tool to examine microtextures of quartz sand-sized grains. Micron 110, 36–45.
Takashimizu, Y., Iiyoshi, M., 2016. New parameter of roundness R: circularity corrected by aspect ratio. Prog. Earth Planet. Sci. 3, 1–16.
Vos, K., Vandenberghe, N., Elsen, J., 2014. Surface textural analysis of quartz grains by scanning electron microscopy (SEM): from sample preparation to environmental interpretation. Earth Sci. Rev. 128, 93–104.
Wadell, H., 1932. Volume, shape, and roundness of rock particles. J. Geol. 40, 443–451.
Wang, G., Li, J., Ravi, S., Van Pelt, R.S., Costa, P.J., Dukes, D., 2017. Tracer techniques in aeolian research: approaches, applications, and challenges. Earth Sci. Rev. 170, 1–16.
Williams, M.A.J., Clarke, M.F., 1984. Late Quaternary environments in north-central India. Nature 308, 633–635.
Wu, C., Qian, P., Zheng, X., Zhou, L., Wang, H., Xu, H., 2020. Quartz grain characteristics of the late Pleistocene hard clay in the Yangtze River delta and implications for sedimentary environment and provenance. Quat. Res. 97, 199–215.
Yadav, S., Chauhan, M.S., Sharma, A., 2007. Characterisation of bio-aerosols during dust storm period in N–NW India. Atmos. Environ. 41, 6063–6073.
Zhou, L., Jiang, Z., Larrasoaña, J.C., Li, S., Liu, Q., Chen, L., Yin, Z., Liu, W., Guan, Y., Zhang, Y., Hu, Y., 2024. Aridity record of the Arabian Peninsula for the last 200 kyr: environmental magnetic evidence from the western equatorial Indian ocean. Quat. Sci. Rev. 341, 108876.